Stem Cell Reports
Article

ISSCR

OPEN ACCESS

Dynamics of *Lgr6*$^+$ Progenitor Cells in the Hair Follicle, Sebaceous Gland, and Interfollicular Epidermis

Anja Füllgrabe,[1] Simon Joost,[1] Alexandra Are,[1] Tina Jacob,[1] Unnikrishnan Sivan,[1] Andrea Haegebarth,[2,7] Sten Linnarsson,[3] Benjamin D. Simons,[4,5,6] Hans Clevers,[2] Rune Toftgård,[1] and Maria Kasper[1,*]

[1]Karolinska Institutet, Department of Biosciences and Nutrition and Center for Innovative Medicine, Novum, 141 83 Huddinge, Sweden
[2]Hubrecht Institute–KNAW (Royal Netherlands Academy of Arts and Sciences) and University Medical Center Utrecht, Uppsalalaan 8, 3584 Utrecht, the Netherlands
[3]Karolinska Institutet, Department of Medical Biochemistry and Biophysics, Scheeles väg 2, 171 77 Stockholm, Sweden
[4]The Wellcome Trust/Cancer Research UK Gurdon Institute, University of Cambridge, Tennis Court Road, Cambridge CB2 1QN, UK
[5]Cavendish Laboratory, Department of Physics, J. J. Thomson Avenue, University of Cambridge, Cambridge CB3 0HE, UK
[6]Wellcome Trust-Medical Research Council Stem Cell Institute, University of Cambridge, Cambridge CB2 1QR, UK
[7]Present address: Bayer Pharma AG, 13353 Berlin, Germany
*Correspondence: maria.kasper@ki.se
http://dx.doi.org/10.1016/j.stemcr.2015.09.013

SUMMARY

The dynamics and interactions between stem cell pools in the hair follicle (HF), sebaceous gland (SG), and interfollicular epidermis (IFE) of murine skin are still poorly understood. In this study, we used multicolor lineage tracing to mark *Lgr6*-expressing basal cells in the HF isthmus, SG, and IFE. We show that these *Lgr6*$^+$ cells constitute long-term self-renewing populations within each compartment in adult skin. Quantitative analysis of clonal dynamics revealed that the *Lgr6*$^+$ progenitor cells compete neutrally in the IFE, isthmus, and SG, indicating population asymmetry as the underlying mode of tissue renewal. Transcriptional profiling of *Lgr6*$^+$ and *Lgr6*$^-$ cells did not reveal a distinct *Lgr6*-associated gene expression signature, raising the question of whether *Lgr6* expression requires extrinsic niche signals. Our results elucidate the interrelation and behavior of *Lgr6*$^+$ populations in the IFE, HF, and SG and suggest population asymmetry as a common mechanism for homeostasis in several epithelial skin compartments.

INTRODUCTION

Skin contains several epithelial structures that undergo constant self-renewal, including the hair follicle (HF), sebaceous gland (SG), and interfollicular epidermis (IFE), making it an ideal organ to study the lineage potential of stem cells in a compartmentalized tissue (Blanpain and Fuchs, 2009; Schepeler et al., 2014). Hair is generated in recurring cycles of growth (anagen), regression (catagen), and resting (telogen) phases of the lower HF part (Müller-Röver et al., 2001). In contrast, the IFE and SG continuously produce cells that differentiate into stratified epithelium or mature sebocytes, respectively (Blanpain and Fuchs, 2014). The murine pilosebaceous unit (PSU), encompassing the HF and SG, has a well-defined anatomy that consists of several subcompartments. The bulge, containing mainly quiescent progenitor cells, and the hair germ, which is in direct contact with the dermal papilla, contribute to the hair lineages during anagen (Greco et al., 2009; Jaks et al., 2008; Rompolas and Greco, 2014). The permanent part of the HF that does not participate in hair regeneration comprises the isthmus, spanning from the bulge to the infundibulum, the junctional zone, which is the upper region of the isthmus adjacent to the SG, and the infundibulum, linking the PSU and the IFE (Schepeler et al., 2014).

Genetic fate-mapping studies using lineage tracing in vivo demonstrated that molecularly defined basal cells that possess stem cell properties reside in most of these regions (Jaks et al., 2010; Kretzschmar and Watt, 2014). Apart from self-renewal, their contribution to other structures seems to remain locally restricted, although contribution of HF cells to SG maintenance during homeostasis has been proposed (Petersson et al., 2011; Schepeler et al., 2014). Because of the large variety of genetic markers used to study the individual stem cell populations, direct comparisons of the results have been difficult. Thus, the interrelation between different stem cell pools within the PSU remains to be elucidated.

The IFE is less well characterized in terms of its cellular heterogeneity and molecular markers. However, the mode of stem cell renewal in the IFE has been a subject of intense research (Doupé and Jones, 2012). Based on genetic lineage tracing studies, it has been proposed that the maintenance of IFE tissue relies on the turnover of a single population of progenitors, which follows a pattern of balanced stochastic fate (Clayton et al., 2007; Doupé et al., 2010). In this paradigm, the division of basal progenitors results in stochastic fate outcome, with cells choosing stochastically between symmetrical duplication, asymmetrical division, and terminal division. However, to achieve homeostasis, the chance of terminal cell division is balanced with the frequency of symmetric duplication so that, on average, cell division results in asymmetric fate outcome. A similar mode of stochastic self-renewal, termed population

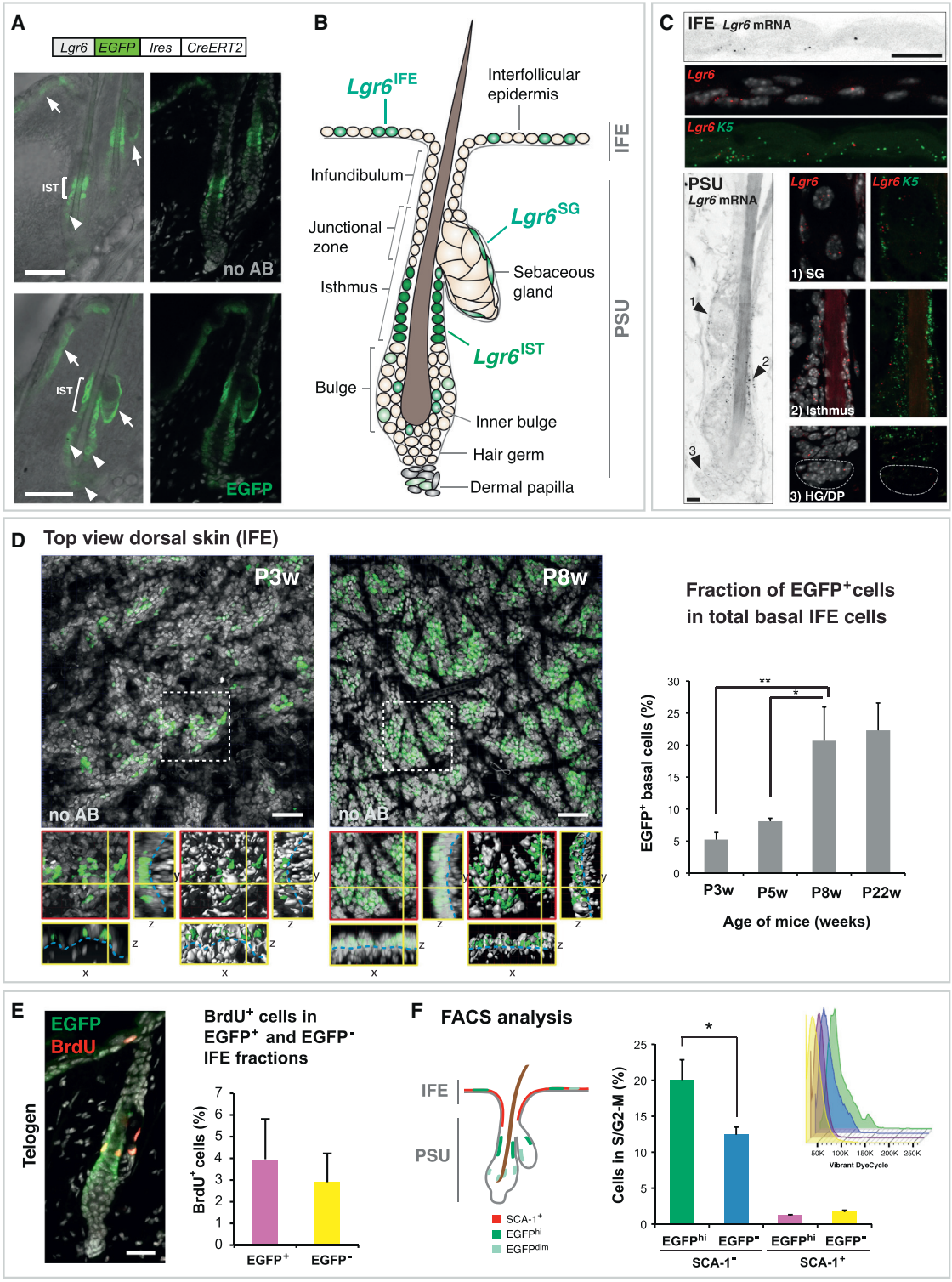

Figure 1. *Lgr6* Expression Pattern in Murine Dorsal Skin

(A) EGFP fluorescence detected by confocal microscopy with EGFP antibody (bottom, n = 5 mice) or without antibody staining (top, no AB, n = 5 mice) in skin of *Lgr6-EGFP-Ires-CreERT2* mice at P3w. EGFP is expressed at high levels in the isthmus (IST), at medium levels in the IFE and SG (arrows), and at low levels in the bulge and dermal papilla (arrowheads).

(legend continued on next page)

asymmetry (Watt and Hogan, 2000), was also observed in other tissues, such as the male germline (Nakagawa et al., 2007), the small intestine (Lopez-Garcia et al., 2010; Snippert et al., 2010b), the esophagus (Doupé et al., 2012), and the stomach (Leushacke et al., 2013). Moreover, a study based on separate targeted promoters provided evidence of proliferative heterogeneity in IFE, with the committed progenitor cell pool underpinned by a second quiescent or slow-cycling stem cell population, which becomes mobilized on injury (Mascré et al., 2012). However, no studies have been performed to determine whether compartments within the PSU are maintained by population asymmetry or whether stem cell self-renewal follows a process of invariant asymmetry in which each and every stem cell division results in an asymmetric fate outcome.

Expression of *Lgr6* (leucine-rich repeat-containing G protein-coupled receptor 6) was initially reported to be a specific marker of stem cells located in the HF isthmus that were thought to give rise to cells of the HF, SG, and IFE lineage (Snippert et al., 2010a). More recent reports have uncovered that *Lgr6* is additionally present in basal cells of the IFE and the SG (Liao and Nguyen, 2014; Page et al., 2013), thus questioning the origin of the *Lgr6*$^+$-derived clones in the first study.

The aim of this study was to define the stem cell properties of the *Lgr6*$^+$ cell populations in the HF, SG, and IFE and understand their interrelation. Tracking the fate of *Lgr6*$^+$ cells using multicolor lineage tracing, the current study revealed that *Lgr6*$^+$ cells in the IFE are able to maintain IFE tissue without contribution from *Lgr6*$^+$ PSU cells. In the isthmus and SG, local *Lgr6*$^+$ cell populations exhibited the potential for long-term maintenance of their respective compartment. Furthermore, quantitative analysis of clonal dynamics revealed that local *Lgr6*$^+$ progenitors renew all three compartments through the process of population asymmetry. Finally, genome-wide mRNA profiling uncovered that the transcriptome of *Lgr6*$^+$ keratinocytes is mainly determined by the cellular location, rather than by a gene signature specific for *Lgr6*$^+$ cells.

RESULTS

Characterization of *Lgr6* Expression in Murine Dorsal Skin

As a prerequisite to investigating how *Lgr6*$^+$ keratinocytes produce HF, IFE, and SG, we first characterized *Lgr6* expression in the skin using *Lgr6-EGFP-Ires-CreERT2* knockin mice (Snippert et al., 2010a), where EGFP marks cells with active transcription of the *Lgr6* locus (*Lgr6*$^+$ cells). A substantial number of *Lgr6*$^+$ cells were found in the basal layer of the isthmus (*Lgr6*^{IST}), IFE (*Lgr6*^{IFE}), and the SG (*Lgr6*^{SG}), with the highest EGFP levels present in the isthmus (Figure 1A), which is consistent with previous findings (Liao and Nguyen, 2014; Page et al., 2013; Snippert et al., 2010a). Additional EGFP antibody staining revealed intermittent, medium- to low-level *Lgr6*-EGFP-expressing cells in the dermal papilla and the inner and outer layer of the bulge (Figures 1A and 1B). Sensitive mRNA in situ detection on WT telogen skin confirmed *Lgr6* transcription in all skin compartments described above (Figure 1C). Throughout the hair cycle, a similar epithelial *Lgr6*-EGFP-expression pattern was observed as in telogen, with additional *Lgr6*-EGFP expression in the proximal part of the early extending and full-grown anagen HF (Figures S1A and S1B).

Lgr6^{IFE} cells of dorsal skin are located exclusively in the basal layer of the epidermis (Figures 1C and 1D). Quantification of *Lgr6*^{IFE} cells by image analysis revealed that the IFE contains approximately 5% *Lgr6*-EGFP-expressing basal cells at postnatal week 3 (P3w). During adolescence, the number of *Lgr6*^{IFE} cells significantly increased, eventually reaching a steady state in adult mice at around 22%

(B) Summary illustrating high (dark green), medium (light green), and low (pale green) *Lgr6*-EGFP expressing cell populations in dorsal telogen skin. Marked cells do not represent absolute positions and numbers of *Lgr6*-EGFP expressing cells.

(C) Representative pattern of *Lgr6* mRNA expression in a telogen HF using single-molecule RNA ISH. Shown are confocal z-stack projections. Co-staining with a *K5*-specific probe indicates the basal identity of *Lgr6*$^+$ cells in the epithelium (n = 3 mice). HG, hair germ; DP, dermal papilla.

(D) Quantification of *Lgr6*^{IFE} cells using image analysis. Projections of flat-mount confocal z stacks recorded in dorsal skin of *Lgr6-EGFP-Ires-CreERT2* mice at P3w and P8w. Magnified sections depict the X, Y, and Z planes, with (right) and without (left) rendering; dashed blue lines indicate basement membrane. The relative number of *Lgr6*^{IFE} cells was determined as the ratio of EGFP$^+$ cells to the total IFE basal cell number ($n \geq 3$ mice for each time point).

(E) Co-staining in skin of *Lgr6-EGFP-Ires-CreERT2* mice with anti-EGFP and anti-BrdU antibodies at P3w telogen; BrdU chased for 2 hr. BrdU-positive cells in *Lgr6*^{IFE} and *Lgr6*$^-$ IFE basal cells were quantified (n = 3 mice, more than 1,000 IFE cells were counted per mouse).

(F) DNA content of keratinocytes from *Lgr6-EGFP-Ires-CreERT2* mice, isolated at P3w telogen, was measured by FACS to determine the percentage of cells in S and G2-M cell-cycle phase in the EGFP^{hi} and EGFP$^-$ fractions of SCA-1$^+$ (IFE/infundibulum) and SCA-1$^-$ (PSU) cells (n = 4 mice). (Inset) Representative Vibrant DyeCycle histograms.

TO-PRO-3 nuclear stain is shown in (A), (D), and (E). DAPI nuclear stain is shown in (C), and without EGFP antibody staining: no AB in (A) and (D). Scale bars represent 50 μm (A and D), 15 μm (C), and 25 μm (E). Data are shown as mean ± SD. Asterisks indicate t test significance level at *p < 0.05 and **p < 0.01. See also Figure S1.

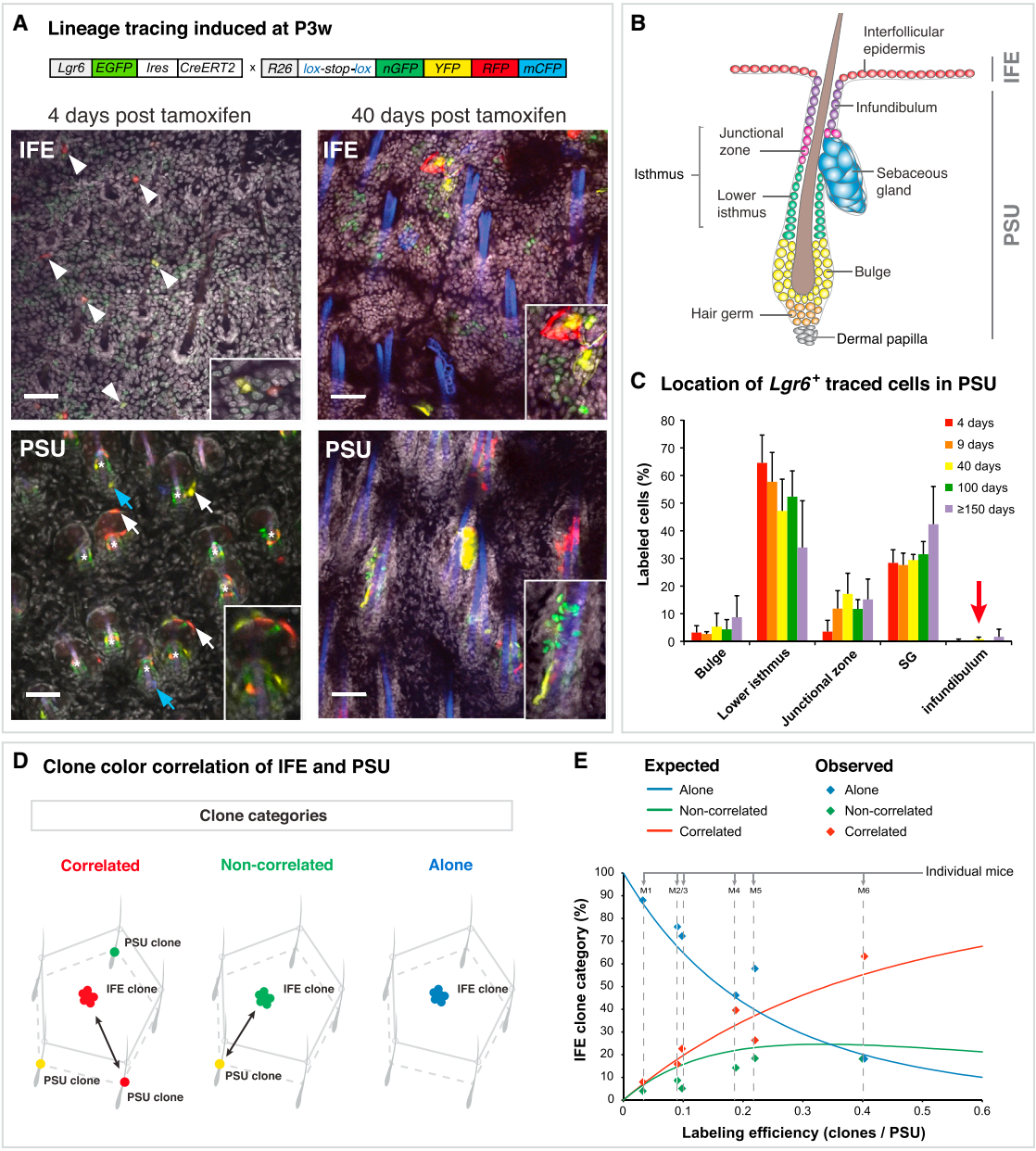

Figure 2. Short- and Long-Term Contribution of *Lgr6-EGFP-Ires-CreERT2/R26R-Confetti* Traced Clones during Homeostasis

(A) Illustrative images for lineage tracing in skin of *Lgr6-EGFP-Ires-CreERT2/R26R-Confetti* mice induced at P3w and traced for 4 or 40 days. Confocal z-stack projections of flat-mount preparations show the IFE and its underlying PSUs. *Lgr6*$^+$ clones are labeled with Confetti colors in nuclear green, cytoplasmic yellow, cytoplasmic red, and membranous blue; *Lgr6*-EGFP expression is cytoplasmic green, and TO-PRO-3 nuclear stain is gray. Hair shafts show autofluorescence in the blue channel. Initial labeling is present in the basal cells of the IFE (arrowheads), isthmus (asterisks), SG (white arrows), and inner bulge (blue arrows). Scale bars represent 50 μm.

(B) Illustration of the epidermal compartments. Confetti-labeled cells were assigned to the respective compartments according to this scheme.

(C) Quantification of Confetti-labeled cell distributions in the PSU after different tracing periods. Notably, cells in the infundibulum were rarely labeled (arrow). The labeled cells in each compartment are given as the percentage of total labeled cells at each time point. In total, 1,308 clones containing 5,082 labeled cells in 1,325 PSUs were analyzed (n = 3 mice per time point). Data are shown as mean ± SD.

(D) Illustration of the assignment of IFE clones, used in (E). First, a random IFE clone was picked, and then all surrounding PSUs were scanned for clones. Three different clone categories were defined: correlated (with PSU clone of the same color), non-correlated (with PSU clone of a different color), or alone (no labeled PSU in the vicinity).

(legend continued on next page)

(Figure 1D). To quantify *Lgr6*^{IFE} cells by fluorescence-activated cell sorting (FACS), we stained isolated keratinocytes of *Lgr6-EGFP-Ires-CreERT2* mice with SCA-1 and CD49f (integrin alpha 6) antibodies (Jensen et al., 2008) to discriminate *Lgr6*^{IFE} cells (SCA-1^{+}) from *Lgr6*$^{+}$ keratinocytes of the PSU (*Lgr6*^{PSU}) (SCA-1^{-}). The FACS analysis confirmed that the fraction of EGFP^{hi} cells increased from P3w to P8w in both SCA-1^{+} and SCA-1^{-} fractions (Figure S1C).

Because *Lgr6*$^{+}$ cells are found in rapidly proliferating epidermal regions, such as the isthmus and the hair germ upon anagen entry (Figure S1A) (Lien et al., 2014), we investigated whether *Lgr6*^{IFE} cells differed from *Lgr6*$^{-}$ IFE cells in regard to cell-cycle activity. A 2-hr bromodeoxyuridine (BrdU) pulse during telogen revealed a comparable BrdU^{+} cell fraction in *Lgr6*^{IFE} and *Lgr6*$^{-}$ IFE cells, suggesting similar proliferation rates at the population level (Figure 1E). Analysis of the DNA content by FACS confirmed that *Lgr6*^{IFE} cells do not significantly differ from *Lgr6*$^{-}$ IFE cells in cell-cycle activity (Figure 1F). FACS analysis further disclosed a higher cell-cycle activity in *Lgr6*^{PSU} cells compared with *Lgr6*$^{-}$ PSU cells (Figure 1E), likely reflecting the abundance of *Lgr6*$^{+}$ cells in the more proliferative isthmus area relative to the rest of the telogen HF (Figure S1D).

Overall, *Lgr6* expression marks a subset of basal cells in several epithelial skin compartments and is not generally correlated with cell division.

The *R26R-Confetti* Reporter Labels Three Basal *Lgr6*$^{+}$ Populations

In order to investigate whether the different *Lgr6*$^{+}$ populations in the dorsal epidermis are able to maintain tissue within their local compartment, we employed a lineage tracing strategy in *Lgr6-EGFP-Ires-CreERT2* mice combined with *R26R-Confetti* multicolor reporter mice (Snippert et al., 2010b). After Cre-mediated recombination, one of four fluorescent marker proteins will be expressed, generating nuclear green, cytoplasmic yellow, cytoplasmic red, or membranous blue cells (Confetti-labeled cells). This allows discrimination between the clonal progeny of individual cells. Fluorescent labeling and tracing of *Lgr6*$^{+}$ cells were induced at first telogen (P3w) by topical application of a single tamoxifen dose. Subsequently, Confetti-labeled cells and entire clones were mapped to the different epidermal compartments, defining cohesively connected cells in the same color as single clone (Figures 2A and 2B). Initial labeling, 4 days after induction, revealed single- or two-cell clones in the basal layer of the IFE, isthmus, SG, and the inner bulge (Figure 2A). Notably, initial labeling in the bulge was restricted to the inner layer, where cells have been shown to be post-mitotic (Hsu et al., 2011). Thus, when using the *R26R-Confetti* reporter, we assume that all expanding *Lgr6*$^{+}$-derived clones originated either from the isthmus, SG, or IFE basal layer. Untreated *Lgr6-EGFP-Ires-CreERT2/R26R-Confetti* mice did not show any clone development at 1 year of age (Figure S2A). Moreover, tamoxifen treatment induced a delay in anagen entry of at least 10 days (Figure S2B), and at all time points, PSUs in telogen were analyzed. Following the tracing pattern over different time periods, up to 1 year, revealed that *Lgr6*$^{+}$-traced cells were present in the IFE, the isthmus including the junctional zone, the SG, and the bulge, whereas the infundibulum was very rarely labeled (Figure 2C). We frequently detected clones in the isthmus, SG and IFE, respectively, without any connection to another compartment (Figure 2A; 40-days PSU [yellow SG, green isthmus]), implying that all three compartments contain their own resident *Lgr6*$^{+}$ stem or progenitor cells. However, this observation does not exclude that an *Lgr6*$^{+}$ population, while maintaining itself, also contributes to another *Lgr6*$^{+}$ compartment. We thus sought to investigate the clonal relationship between the different *Lgr6*$^{+}$ populations next.

Isthmus, SG, and IFE Harbor Resident Self-Renewing *Lgr6*$^{+}$ Populations

It has been shown that cells originating in the HF bulge area can contribute to the infundibulum and the IFE when challenged with a wound environment (Brownell et al., 2011; Ito et al., 2005; Kasper et al., 2011; Levy et al., 2005). Investigating *Lgr6*^{PSU}-derived clones in closing wounds (5-days post-wounding) and healed scar areas ($\geq$36 days post-wounding) demonstrated that *Lgr6*^{PSU} progeny also leave a Confetti-trace in the infundibulum when recruited to the IFE (Figures S2C and S2D). Importantly, the absence of such a tracing pattern in healthy skin strongly argues against a continuous flux of *Lgr6*^{PSU}-derived cells to the IFE.

To rule out that Confetti-labeled *Lgr6*^{PSU} cells migrate to the IFE during tissue homeostasis without leaving a Confetti-trace in the infundibulum, we studied the color

(E) Confetti clone color correlation between IFE and PSU clones. The continuous lines represent the expected percentages for each clone category at given labeling efficiencies (derived via simulation) assuming that IFE and the PSU are independent. Note that the correlated IFE clone category increases steadily with increasing labeling efficiency (x axis). The experimentally determined values (observed) for IFE clone categories were plotted for each individual mouse (M1–M6, values on the y axis add up to 100% for each mouse, see dashed lines). In total, 186 IFE clones and 875 PSUs were analyzed in six mice.
See also Figure S2 and Table S1.

correlation between IFE and PSU clones. In 3D confocal microscopy scans of flat-mount preparations (imaging from the top of the IFE down to the PSU), IFE clones (traced for 40 days up to 1 year) were compared with clones in the PSUs located around an IFE clone in an ~175-μm radius (Figure 2D). IFE clones were then categorized as "correlated" (with PSU clone of the same color in the vicinity), "non-correlated" (with PSU clone of a different color in the vicinity), or "alone" (no labeled PSU in the vicinity) (Figure 2D). If IFE clones were derived from PSU cells, all IFE clones should have a color-matched clone in one of their surrounding PSUs. However, even if IFE clones are independent from PSU clones, it is expected that some color-matched clones will appear by chance due to the color limitation. These expected frequencies are dependent on the labeling efficiency and the actual occurrence of Confetti-clone colors in IFE and PSU, which vary between individual mice. Thus, we used a simulation strategy (see Supplemental Experimental Procedures) to determine the expected frequencies of correlated, non-correlated, and alone clones under the assumption that there is no cellular exchange between the IFE and the PSU. We then compared observed and expected frequencies and found that, irrespective of labeling efficiency, the observed frequencies matched the expected correlations for independent clones within 2 SDs (Figure 2E; Table S1). This color correlation analysis indicates that the IFE and the PSU clones are independent, which was further confirmed through an alternative resampling strategy estimating the expected color correlations within each mouse independently (Figure S2E; Supplemental Experimental Procedures). In summary, *Lgr6*^{PSU} cells do not contribute to *Lgr6*$^{+}$-derived clones in the IFE, demonstrating that the IFE harbors a long-term self-renewing *Lgr6*$^{+}$ population.

To investigate the clonal relationship between the *Lgr6*^{IST} and *Lgr6*^{SG} populations, we compared all SG clones, traced for 40 days up to 1 year, to clones in the isthmus of the respective PSUs (Figures S2F and S2G). SG clones were then categorized as correlated (isthmus clone of the same color), non-correlated (isthmus clone of a different color), or alone (no clone in the isthmus) (Figure S2G). After applying the same resampling strategy as for the IFE, the results suggest that the *Lgr6*^{SG} and *Lgr6*^{IST} populations are maintained independently. However, a minor cellular exchange between the isthmus and SG may not be ruled out (Figure S2F).

Lgr6^{IFE}, *Lgr6*^{IST}, and *Lgr6*^{SG} Clone Dynamics Show the Hallmarks of Neutral Competition

Since *Lgr6*^{IFE}, *Lgr6*^{IST}, and *Lgr6*^{SG} populations all exhibited long-term clone survival, we wanted to assess the mode of stem cell renewal within the three epidermal compartments. In homeostasis, modes of stem cell self-renewal can be grouped into two classes of model: invariant asymmetry (in which each and every stem cell division results in strictly asymmetric fate outcome) and population asymmetry (where stochastic stem cell loss through differentiation is perfectly compensated by stem cell duplication) (Simons and Clevers, 2011). In contrast to invariant asymmetry, where clone number and size are predicted to remain approximately constant over time, tissues maintained by population asymmetry are characterized by an increase in average clone size while their number steadily diminishes so that the overall size of the labeled population remains constant. Furthermore, within this dynamics, the clone size distribution is predicted to acquire a hallmark scaling behavior, in which the chance of finding a clone with a size some multiple of the average remains constant (Klein and Simons, 2011).

Based on this characterization, we analyzed the Confetti-clone frequency and clone size of IFE clones, isthmus clones, and SG clones after different tracing times starting at P3w (Figures 3 and S3; allocation of clones is described in Supplemental Experimental Procedures). The numbers of analyzed mice for each time point, including counted clones and the total number of labeled cells, are listed in Table S2. Significantly, in all skin compartments, the overall clone frequency still increased from 4 to 9 days of tracing, with the highest fold change seen in the IFE (Figures 3A–3C, left). This delay in clone emergence may be due to prolonged tamoxifen/Cre activity on the *R26R-Confetti* construct or a slow accumulation of reporter protein levels (expression of membranous CFP and nuclear GFP was delayed beyond day 4; see Table S2).

Following IFE clone development from 9 days onward revealed a steady decline in clone number combined with an increase in average clone size so that the overall number of labeled cells stayed approximately constant (Figures 3A and S3A). This clone fate behavior in dorsal skin matches that described for tail, ear, and paw IFE (Clayton et al., 2007; Doupé et al., 2010; Lim et al., 2013) and is suggestive of population asymmetry. Further, the convergence of the *Lgr6*^{IFE}-derived clone size distribution onto an exponential scaling behavior, as predicted by committed progenitor cell dynamics, shows that tissue maintenance follows from neutral competition (Figures 3D, S3B, and S3C) (Clayton et al., 2007). Although the clone size dependence is consistent with a single progenitor cell population, the contribution of a second minority slow-cycling stem cell population cannot be ruled out.

Evaluating the dynamics of *Lgr6*^{IST}-derived clones revealed a similar clone fate behavior as in the IFE, with the clone size converging onto an exponential scaling form and an approximately similar average growth rate (Figures 3B, 3D, S3B, and S3C). Analyses of *Lgr6*^{SG}-derived clones show comparable clone fates, with a decreasing clone

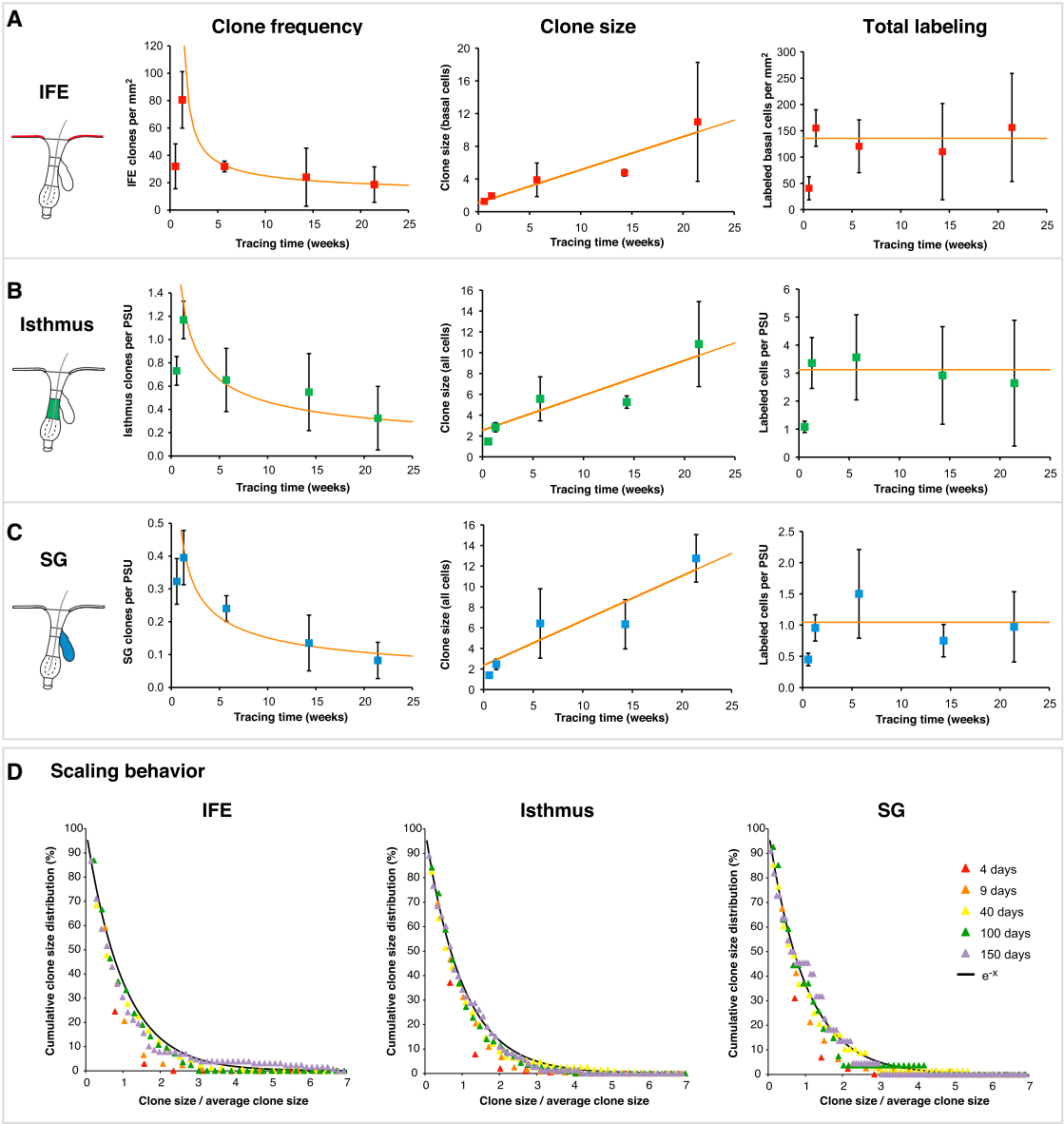

Figure 3. *Lgr6-EGFP-Ires-CreERT2/R26R-Confetti* Clone Dynamics in the IFE, Isthmus, and SG

Lgr6-EGFP-Ires-CreERT2/R26R-Confetti tracing was induced in telogen at P3w, and clone frequency, size, and the number of labeled cells were counted in the IFE, isthmus, and SG over time.

(A–C) Observed clone data are shown as mean ± SD of three mice, and the orange lines show the best fit according to the neutral competition model. (A) Average number of IFE clones per mm^2, average clone size of basal cells, and average number of labeled basal cells per mm^2 IFE for the respective time points. (B) Average number of isthmus clones per PSU, average clone size, and average number of labeled cells per PSU for the respective time points. (C) Average number of SG clones per PSU, average clone size, and average number of labeled SG cells per PSU for the respective time points.

(D) Scaling behavior of *Lgr6*$^+$-derived IFE, isthmus, and SG clones represented by the cumulative clone size distribution. For each time point, clone sizes from three mice were pooled and divided by the average clone size of the respective time point. Theory predicts that if stem cell self-renewal follows from population asymmetry the probability of finding a surviving clone with n/(average n(t)) cells remains constant over time. Black line denotes the scaling curve $F(x) = e^{-x}$.

See also Figure S3 and Table S2.

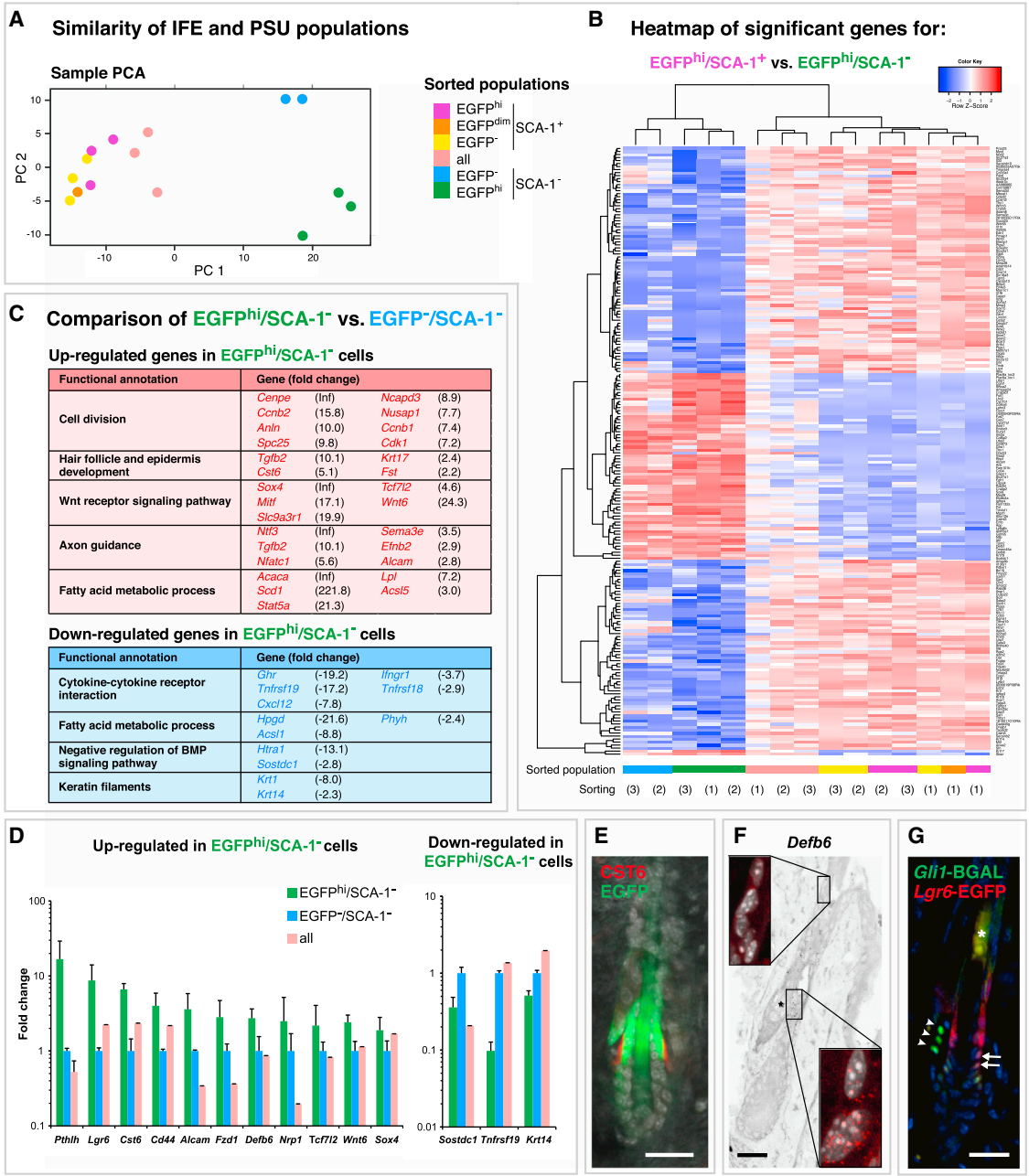

Figure 4. Gene Expression Profiles of *Lgr6*^{IFE} and *Lgr6*^{PSU} Cell Populations

(A) Two-dimensional principle component analysis (PCA) of sorted cell populations based on the 500 genes with the highest variance demonstrates a clear separation between SCA-1^{+} (IFE/infundibulum) and SCA-1^{-} (PSU) cells. Three independent sortings were performed. See Figure S4A for detailed illustration of the location and the gating strategy used for each cell population.

(B) Heatmap of the most differentially expressed genes between EGFP^{hi}/SCA-1^{+} and EGFP^{hi}/SCA-1^{-} cells, including hierarchical clustering of all sorted cell populations (biological replicates indicated by digits), illustrating the distinct PSU and IFE signatures.

(C) Functional annotation analysis of genes significantly upregulated or downregulated in EGFP^{hi} cells compared with EGFP^{-} cells in the SCA-1^{-} fraction. Functional groups, genes, and their fold changes are shown (Inf: no reads were counted in the reference population).

(D) Real-time PCR analysis of selected upregulated or downregulated genes in EGFP^{hi} cells compared with EGFP^{-} cells in the SCA-1^{-} fraction. Data are shown as mean of two or more biological replicates ± SD.

(E) Co-staining in telogen skin of *Lgr6-EGFP-Ires-CreERT2* mice with anti-EGFP (green), anti-CST6 (red), and TO-PRO-3 nuclear stain shows co-localization of *Lgr6*-EGFP and CST6 expression in the lower isthmus (n = 3 mice).

(legend continued on next page)

number and an increasing clone size and exponential scaling behavior (Figures 3C, 3D, S3B, and S3C). The fact that both *Lgr6*^{IST} and *Lgr6*^{SG} clone dynamics conform to the predictions of the committed progenitor model again denotes that a potential cellular exchange between isthmus and SG must be small enough not to affect the clone size distribution.

In summary, the clonal fate data from the IFE, isthmus, and SG suggest population asymmetry as the mode of stem cell renewal in all three compartments.

Lgr6^{+} Keratinocytes of the IFE and PSU Do Not Share a Common Gene Expression Signature

Finally, we asked whether *Lgr6*^{IFE} and *Lgr6*^{PSU} cells share a certain transcriptional signature that is unique to *Lgr6*-expressing cells. We isolated *Lgr6*$^{+}$ and *Lgr6*$^{-}$ keratinocytes from the SCA-1^{+} and the SCA-1^{-} fraction using live-cell sorting (Figure S4A) and performed mRNA sequencing (RNA-seq) analysis of the sorted keratinocyte populations. The purity and the correct identity of the populations were validated based on read counts and real-time PCR (Figures S4B–S4D). A comparison of the global expression profiles using Pearson correlation (Figure S4E) and principal component analysis (PCA) (Figure 4A) revealed that the *Lgr6*$^{+}$ populations do not show a high degree of similarity to each other. Moreover, we did not find significant differentially regulated genes when comparing all EGFP^{hi} populations to the EGFP^{-} populations. Hierarchical clustering based on the most differentially expressed genes between the two EGFP^{hi} populations revealed that EGFP^{hi}/SCA-1^{+} cells display a clear IFE identity while EGFP^{hi}/SCA-1^{-} cells present a signature more similar to their neighboring HF and SG cells (Figures 4B and S4F). This indicates that the transcription profile of *Lgr6*$^{+}$ cells is markedly influenced by the local environment.

Transcriptional Comparison between *Lgr6*$^{+}$ and *Lgr6*$^{-}$ Cells within the PSU

PCA indicated that *Lgr6*^{PSU} and *Lgr6*$^{-}$ PSU cells have distinct characteristics (see Figure 4A). The most pronounced difference of *Lgr6*^{PSU} cells compared with *Lgr6*$^{-}$ PSU cells was the upregulation of a gene cluster related to cell division (Figure 4C), which is in line with the cell-cycle analysis (Figure 1F). Since LGR6 is implicated as an R-spondin receptor and thus a potential modulator of the Wnt pathway (de Lau et al., 2011), we had a closer look at the expression of Wnt signaling-related genes and found several Wnt-pathway associated genes such as *Wnt6*, *Fzd1*, *Sox4*, *Tcf7l2* upregulated in *Lgr6*^{PSU} cells (Figures 4C and 4D). Interestingly, several genes associated with nerve fiber development, and axon morphogenesis were upregulated in *Lgr6*^{PSU} cells, such as *Alcam*, *Sema3e*, *Ntf3*, and *Nrp1* (Figures 4C and 4D), which suggest an interaction of *Lgr6*$^{+}$ cells with nerve fibers, as recently denoted (Liao and Nguyen, 2014). The most prominently downregulated genes in *Lgr6*^{PSU} cells were associated with cytokine receptors (*Tnfrsf19* and *Cxcl12*) and negative regulation of BMP signaling (*Sostdc1* and *Htra1*) (Figures 4C and 4D). Since the *Lgr6*^{PSU} likely contains a mixture of *Lgr6*^{IST} and *Lgr6*^{SG}, also SG-associated genes such as *Scd1* were found to be upregulated (Figure 4C). However, many genes that were highly enriched in *Lgr6*^{PSU} cells have previously been mapped to the isthmus, like parathyroid hormone-related protein (*Pthlh*) (Cho et al., 2003), neurotrophin-3 (*Ntf3*) (Botchkarev et al., 1998), *Cd44* (Jensen et al., 2008), and CST6 (Veniaminova et al., 2013). For validation, we stained P3w telogen skin for CST6, *Defb6*, and beta-galactosidase (under the control of the *Gli1* promoter; Brownell et al., 2011) (Figures 4E–4G). CST6 was found to be co-localized with *Lgr6*-EGFP in the lower part of the isthmus (Figure 4E). *Defb6* expression was detected by mRNA in situ hybridization (ISH) in the isthmus (including the junctional zone), highlighting a potential role of the isthmus for immune regulation in the PSU (Figure 4F). Finally, using *Lgr6-EGFP-Ires-CreERT2/Gli1-LacZ* mice, we detected a partial overlap of the *Lgr6*$^{+}$ and *Gli1*$^{+}$ populations in the lower isthmus closest to the bulge (Figure 4G), as has been speculated previously (Kretzschmar and Watt, 2014). In summary, we could not detect a significant set of genes that is generally co-expressed with *Lgr6*; however, we could highlight genes that are differentially expressed in the *Lgr6*^{PSU} when compared with the rest of the basal PSU cells.

DISCUSSION

Combining multicolor lineage tracing in intact tissue with confocal microscopy, we were able to trace *Lgr6*$^{+}$ epidermal progenitor cells within the native 3D environment. We found that *Lgr6*^{IFE} cells give rise to long-term IFE clones

(F) *Defb6* mRNA detected by single-molecule RNA ISH, and presented as confocal z-stack projection image. Insets are magnifications of isthmus and infundibulum. Asterisk marks SG devoid of *Defb6* (n = 3 mice).
(G) Co-staining in telogen skin of *Lgr6-EGFP-Ires-CreERT2/Gli1-LacZ* mice with anti-EGFP (red), anti-BGAL (green), and DAPI nuclear stain shows a partial overlap of the *Lgr6*$^{+}$ and *Gli1*$^{+}$ populations in the lower isthmus (arrows). Arrowheads indicate BGAL-expression in *Gli1*$^{+}$ cells in the surrounding stroma. Asterisk marks unspecific fluorescence of the hair shaft (n = 3 mice).
Scale bars represent 25 μm (E–G). See also Figure S4.

without contribution from *Lgr6*^{PSU} cells. This is in line with previous work, supporting a PSU-independent maintenance of the IFE during homeostasis (Ghazizadeh and Taichman, 2001; Ito et al., 2005; Levy et al., 2005; Nowak et al., 2008; Page et al., 2013). Moreover, we sporadically observed monoclonal conversion in the three compartments harboring resident *Lgr6*$^{+}$ progenitor cells and found further evidence for their independence using simulation of the Confetti-color correlation, which supports the notion of a compartmentalized epidermis (Schepeler et al., 2014).

The clonal dynamics of *Lgr6*^{IFE} progeny in dorsal skin matched those of prior experiments performed in tail, ear, and paw epidermis, indicating that population asymmetry is the underlying mode of tissue renewal (Clayton et al., 2007; Doupé et al., 2010; Lim et al., 2013; Mascré et al., 2012). In contrast to previous studies where the genetic labeling system targeted all IFE basal progenitors, albeit with variable efficiency, the *Lgr6-EGFP-Ires-CreERT2* system targets only a subset of basal cells that display similar proliferation rates at the population level as the *Lgr6*$^{-}$ IFE cells. Based on *Lgr6*$^{+}$ clone dynamics, we provide evidence that in three distinct compartments, formed by a continuous epithelial basal layer, tissue renewal follows from neutral competition regardless of specific differentiation programs (e.g., stratified epithelium or mature sebocytes). At 14 weeks of tracing, we observed a consistent outlier behavior across all compartments, where the average clone size was lower than expected. This is interesting because it could reflect an ongoing tissue expansion during the postnatal development (visible due to labeling induction before adulthood), where a first wave of cellular overproduction is followed by a degree of uncompensated loss after postnatal development. However, this should not impact the qualitative conclusions drawn about *Lgr6*$^{+}$ progenitor cell dynamics (Clayton et al., 2007).

When analyzing *Lgr6*-EGFP expression, we detected an increase of *Lgr6*^{IFE} cells during postnatal development, which raises key questions for future studies. For example, such a significant increase could be achieved by selective expansion of an *Lgr6*$^{+}$ population, which remains *Lgr6*$^{+}$ and grows (clonal dominance), or by expansion of a niche that drives *Lgr6* expression. The clonal data do not suggest that clonal dominance leads to this increase, favoring the possibility that *Lgr6* expression is influenced by extrinsic factors that are established for example during adolescence. As reported previously, cutaneous nerve fibers may supply signals defining the *Lgr6* expression pattern (Liao and Nguyen, 2014). Supporting this notion, we found genes related to neural development specifically expressed in *Lgr6*^{PSU} cells, where increased expression of *Efnb2* and *Sema3e*, and downregulation of *Cxcl12*, suggest a potential role of *Lgr6*$^{+}$ cells in active axon repulsion (Guan and Rao, 2003). Nerve signals, however, may not explain *Lgr6* expression in the extending anagen HF, inner bulge, and SG. Increased *Lgr6* expression upon anagen entry was recently shown to be governed by beta-catenin (Lien et al., 2014), and we confirmed *Lgr6*-EGFP upregulation in the hair germ during anagen entry in *Lgr6-EGFP-Ires-CreERT2* mice. Yet, canonical Wnt signaling is unlikely to regulate *Lgr6* expression in the SG as beta-catenin signaling suppresses the SG phenotype (Silva-Vargas et al., 2005), and expression of dominant-negative LEF1 protein leads to upregulation of *Lgr6* along with other SG progenitor markers (Petersson et al., 2011). Thus, the regulation of *Lgr6* transcription seems rather complex and further work is needed to uncover all influential signals and pathways.

In summary, the presence of *Lgr6*$^{+}$ cells in multiple skin compartments offered the unique possibility to simultaneously follow the fates and dynamics of epidermal progenitors influenced by distinct cell-intrinsic and environmental cues. Our results support that healthy tissue is renewed in a compartmentalized fashion and highlight the robustness of stochastic stem cell renewal to varying microenvironments.

EXPERIMENTAL PROCEDURES

Mice

All animal experiments were performed in accordance with the Swedish legislation and were approved by the Stockholm South Animal Ethics Committee. The used knockin strains *Lgr6-EGFP-Ires-CreERT2* (Snippert et al., 2010a), *R26R-Confetti* (Snippert et al., 2010b), and *Gli1-LacZ* (Bai et al., 2002) were described previously and kept on a C57BL/6 background. For lineage tracing, *Lgr6-EGFP-Ires-CreERT2/R26R-Confetti* mice aged 3 weeks (P3w) were treated topically with 1.5-mg 4-hydroxytamoxifen (Sigma) in 100-μl acetone on the dorsal skin. Biopsies were taken 4 days later (P25) to analyze the initial labeling and observe the contribution to wound closure at the biopsied sites. The tracing pattern was analyzed after 4, 9, 40, 100, and 150 days, and 1 year. To mark replicating cells, 0.1-mg/g BrdU was injected intraperitoneally 2 hr before mice were sacrificed.

Sample Preparation and Microscopy for Confetti Clone Detection

Dorsal hair was removed with hair removal cream (Veet), and skin pieces ~1–2 cm^2 were fixed in 4% paraformaldehyde (PFA) for 20 min. Subcutaneous fat was removed with a scalpel, and small skin pieces (~10–20 mm^2) were stained with TO-PRO-3 (Invitrogen) in PBS overnight. The skin was mounted flat on a cover glass and overlaid with Pro-Long Gold mounting medium (Invitrogen). Confocal imaging is described in detail in Supplemental Experimental Procedures. To detect Confetti IFE and PSU labels in the same area, z-stack images spanning the depth of the PSU were recorded with a confocal plane distance of 4 μm. Projections of z-stack planes were generated using ImageJ.

Confetti Clone Definition and Color Correlation

Single Confetti clones were defined as coherent labels of the same color. For clone color correlation of the IFE, all PSUs within a radius of 150–200 μm were evaluated, and for SGs, the respective isthmus of the same PSU was analyzed. Detailed descriptions of clone categorization as well as the simulation and resampling strategies are provided in Supplemental Experimental Procedures. For determining the clone dynamics, we counted the number of basal cells per IFE clone and measured the area of IFE clones in z projections. In the isthmus and SG, the total number of cells per clone was quantified. The expected curves for the clone frequency were modeled to the best fit, based on the formulas given in (Klein and Simons, 2011). The first data point is shown but was excluded from the calculations since not all labels had been revealed.

Immunofluorescence Staining and RNA ISH

For immunofluorescence (IF), the following primary antibodies were used: rabbit anti-EGFP (Invitrogen/A-11122, 1:500), rat anti-BrdU (Serotec/OBT0030G, 1:400), rabbit anti-CST6 (Aviva Systems Biology/ARP53533_P050, 1:100), and chicken anti-β-galactosidase (Abcam/ab9361, 1:400). ISH was performed using an RNAscope Fluorescent Multiplex Kit (Advanced Cell Diagnostics) according to the manufacturer's instructions. IF was performed on PFA-fixed horizontal whole-mount dorsal skin preparations and ISH on PFA-fixed paraffin-embedded dorsal skin sections (Supplemental Experimental Procedures).

Keratinocyte Isolation and FACS Analysis

Keratinocytes were isolated from P3w mice as described previously, pooling cells from two to three mice per experiment (Jaks et al., 2008). Cells were stained with AlexaFluor647-conjugated anti-CD49f (integrin alpha 6; 1:20) and PE-Cy7-conjugated anti-SCA-1 (1:15) antibodies (both BD Biosciences). For negative control, cells were stained with the respective isotype control antibodies (AlexaFluor647 Rat IgG2a, and PE-Cy7 Rat IgG2a, BD Biosciences). Staining with 7-AAD (BD biosciences) was used to exclude dead cells. To measure the cell cycle, cells were treated with verapamil (Sigma; 100 mM final concentration) for 15 min at 37°C before Vybrant DyeCycle Violet Stain (Molecular Probes) was added (5 μM final concentration), and cells were incubated for another 30 min. Cells were analyzed on a BD LSRFortessa. FACS data were analyzed using FlowJo software (Tree Star).

Cell Sorting and RNA Isolation

Keratinocytes stained for CD49f, SCA-1, and 7-AAD were sorted using a FACSAria III (BD). *Lgr6*^{IFE} cells were defined as the CD49f^{high}, SCA-1^{high}, and EGFP^{high} fraction, and *Lgr6*^{PSU} cells as the CD49f$^{high+dim}$, SCA-1^{-}, and EGFP^{high} fraction (Jensen et al., 2008). We also collected the respective *Lgr6*$^{-}$ PSU (CD49f^{high}, SCA-1^{-}, and EGFP^{-}), *Lgr6*$^{-}$ IFE/infundibulum (CD49f^{high}, SCA-1^{high}, and EGFP^{-}) and "all" (containing a mix of all four) basal populations. One hundred thousand cells were collected for each population. RNA was isolated from sorted keratinocytes by combining the RNA-containing aqueous phase extract using RNA-Bee (Amsbio) with the RNAaqueous-Micro Kit (Ambion). RNA integrity was measured using an Agilent 2100 Bioanalyzer Pico Chip or a 2200 TapeStation High Sensitivity R6K Screen Tape. The RNA integrity number of all samples was higher than 8.5.

RNA Sequencing and Real-Time PCR

RNA samples from three independent sortings (S1, S2, S3) were analyzed by RNA sequencing. The procedure was performed according to the STRT4 protocol (Islam et al., 2012), starting with 1 ng total RNA per sample in duplicates. Sequence data were preprocessed using the pipeline established in the Linnarsson lab (Islam et al., 2012). Briefly, reads were aligned to mouse genome (mm10 assembly), maintaining only uniquely aligned reads. Reads falling into annotated Refseq gene regions were summed into a raw read count matrix (Islam et al., 2012). We identified differentially expressed genes using DESeq (Anders and Huber, 2010) and SAM-seq (Li and Tibshirani, 2013), with standard parameters in R/Bioconductor environment. In Figure 4B, we displayed differentially expressed genes with a DESeq adjusted p value below 0.1 and a fold change above 2. Functional analyses defining Gene Ontology (GO) category clusters of significant genes were performed with the DAVID online tool.

To validate RNA-seq results, real-time PCR was performed on the same RNA samples used for sequencing after pre-amplification of the cDNA with gene-specific, nested primers. The raw C_T values were normalized to the mean of *Hprt1* and *Rplp0*. Detailed description is provided in Supplemental Experimental Procedures, and primer sequences and PCR conditions are given in Tables S3 and S4.

ACCESSION NUMBERS

The accession number for the RNA-sequencing data reported in this paper is ArrayExpress: E-MTAB-3533.

SUPPLEMENTAL INFORMATION

Supplemental Information includes Supplemental Experimental Procedures, four figures, and four tables and can be found with this article online at http://dx.doi.org/10.1016/j.stemcr.2015.09.013.

AUTHOR CONTRIBUTIONS

A.F., R.T., and M.K. conceived the study. A.F. and M.K. designed the experiments. A.F., A.A., S.J., T.J., and U.S. performed experiments. S.L. provided sequencing platform. A.F., S.J., U.S., and B.D.S. analyzed the data. A.H. and H.C. generated and provided mouse strains. A.F. and M.K. wrote the manuscript with critical input from all authors.

ACKNOWLEDGMENTS

We thank Åsa Bergström for technical help and assistance with mouse strains, Viljar Jaks for his help with FACS analysis, and Anna Johnsson and Peter Lönnerberg for conducting RNA-seq. This work was supported by grants from the Swedish Cancer Society, Swedish Research Council, H&G Jeanssons Foundation, Swedish Foundation for Strategic Research and Ragnar Söderberg Foundation (to M.K.), the Swedish Cancer Society, Swedish

Research Council (to R.T.), the European Molecular Biology Organization (to A.H.), the Swedish Research Council (STARGET to M.K. and S.L.), and the Wellcome Trust (grant number 098357/Z/12/Z to B.D.S.). A.F. was supported by the EU FP7 ITN Healing Network. Parts of this study were performed at the (1) Live Cell Imaging unit, Department of Biosciences and Nutrition, Karolinska Institutet, Sweden, supported by grants from the Knut and Alice Wallenberg Foundation, the Swedish Research Council, the Center for Innovative Medicine and the Jonasson donation to the School of Technology and Health, Royal Institute of Technology, Sweden, and (2) Wallenberg Institute for Regenerative Medicine Flow Cytometry Facility financed by Knut and Alice Wallenberg Foundation, Karolinska Institutet, Huddinge, Sweden.

Received: August 14, 2014
Revised: September 15, 2015
Accepted: September 16, 2015
Published: October 22, 2015

REFERENCES

Anders, S., and Huber, W. (2010). Differential expression analysis for sequence count data. Genome Biol. *11*, R106.

Bai, C.B., Auerbach, W., Lee, J.S., Stephen, D., and Joyner, A.L. (2002). Gli2, but not Gli1, is required for initial Shh signaling and ectopic activation of the Shh pathway. Development *129*, 4753–4761.

Blanpain, C., and Fuchs, E. (2009). Epidermal homeostasis: a balancing act of stem cells in the skin. Nat. Rev. Mol. Cell Biol. *10*, 207–217.

Blanpain, C., and Fuchs, E. (2014). Stem cell plasticity. Plasticity of epithelial stem cells in tissue regeneration. Science *344*, 1242281.

Botchkarev, V.A., Welker, P., Albers, K.M., Botchkareva, N.V., Metz, M., Lewin, G.R., Bulfone-Paus, S., Peters, E.M., Lindner, G., and Paus, R. (1998). A new role for neurotrophin-3: involvement in the regulation of hair follicle regression (catagen). Am. J. Pathol. *153*, 785–799.

Brownell, I., Guevara, E., Bai, C.B., Loomis, C.A., and Joyner, A.L. (2011). Nerve-derived sonic hedgehog defines a niche for hair follicle stem cells capable of becoming epidermal stem cells. Cell Stem Cell *8*, 552–565.

Cho, Y.M., Woodard, G.L., Dunbar, M., Gocken, T., Jimènez, J.A., and Foley, J. (2003). Hair-cycle-dependent expression of parathyroid hormone-related protein and its type I receptor: evidence for regulation at the anagen to catagen transition. J. Invest. Dermatol. *120*, 715–727.

Clayton, E., Doupé, D.P., Klein, A.M., Winton, D.J., Simons, B.D., and Jones, P.H. (2007). A single type of progenitor cell maintains normal epidermis. Nature *446*, 185–189.

de Lau, W., Barker, N., Low, T.Y., Koo, B.K., Li, V.S., Teunissen, H., Kujala, P., Haegebarth, A., Peters, P.J., van de Wetering, M., et al. (2011). Lgr5 homologues associate with Wnt receptors and mediate R-spondin signalling. Nature *476*, 293–297.

Doupé, D.P., and Jones, P.H. (2012). Interfollicular epidermal homeostasis: dicing with differentiation. Exp. Dermatol. *21*, 249–253.

Doupé, D.P., Klein, A.M., Simons, B.D., and Jones, P.H. (2010). The ordered architecture of murine ear epidermis is maintained by progenitor cells with random fate. Dev. Cell *18*, 317–323.

Doupé, D.P., Alcolea, M.P., Roshan, A., Zhang, G., Klein, A.M., Simons, B.D., and Jones, P.H. (2012). A single progenitor population switches behavior to maintain and repair esophageal epithelium. Science *337*, 1091–1093.

Ghazizadeh, S., and Taichman, L.B. (2001). Multiple classes of stem cells in cutaneous epithelium: a lineage analysis of adult mouse skin. EMBO J. *20*, 1215–1222.

Greco, V., Chen, T., Rendl, M., Schober, M., Pasolli, H.A., Stokes, N., Dela Cruz-Racelis, J., and Fuchs, E. (2009). A two-step mechanism for stem cell activation during hair regeneration. Cell Stem Cell *4*, 155–169.

Guan, K.L., and Rao, Y. (2003). Signalling mechanisms mediating neuronal responses to guidance cues. Nat. Rev. Neurosci. *4*, 941–956.

Hsu, Y.C., Pasolli, H.A., and Fuchs, E. (2011). Dynamics between stem cells, niche, and progeny in the hair follicle. Cell *144*, 92–105.

Islam, S., Kjällquist, U., Moliner, A., Zajac, P., Fan, J.B., Lönnerberg, P., and Linnarsson, S. (2012). Highly multiplexed and strand-specific single-cell RNA 5′ end sequencing. Nat. Protoc. *7*, 813–828.

Ito, M., Liu, Y., Yang, Z., Nguyen, J., Liang, F., Morris, R.J., and Cotsarelis, G. (2005). Stem cells in the hair follicle bulge contribute to wound repair but not to homeostasis of the epidermis. Nat. Med. *11*, 1351–1354.

Jaks, V., Barker, N., Kasper, M., van Es, J.H., Snippert, H.J., Clevers, H., and Toftgård, R. (2008). Lgr5 marks cycling, yet long-lived, hair follicle stem cells. Nat. Genet. *40*, 1291–1299.

Jaks, V., Kasper, M., and Toftgård, R. (2010). The hair follicle-a stem cell zoo. Exp. Cell Res. *316*, 1422–1428.

Jensen, U.B., Yan, X., Triel, C., Woo, S.H., Christensen, R., and Owens, D.M. (2008). A distinct population of clonogenic and multipotent murine follicular keratinocytes residing in the upper isthmus. J. Cell Sci. *121*, 609–617.

Kasper, M., Jaks, V., Are, A., Bergström, Å., Schwäger, A., Svärd, J., Teglund, S., Barker, N., and Toftgård, R. (2011). Wounding enhances epidermal tumorigenesis by recruiting hair follicle keratinocytes. Proc. Natl. Acad. Sci. USA *108*, 4099–4104.

Klein, A.M., and Simons, B.D. (2011). Universal patterns of stem cell fate in cycling adult tissues. Development *138*, 3103–3111.

Kretzschmar, K., and Watt, F.M. (2014). Markers of epidermal stem cell subpopulations in adult mammalian skin. Cold Spring Harb. Perspect. Med. *4*, a013631.

Leushacke, M., Ng, A., Galle, J., Loeffler, M., and Barker, N. (2013). Lgr5(+) gastric stem cells divide symmetrically to effect epithelial homeostasis in the pylorus. Cell Rep. *5*, 349–356.

Levy, V., Lindon, C., Harfe, B.D., and Morgan, B.A. (2005). Distinct stem cell populations regenerate the follicle and interfollicular epidermis. Dev. Cell *9*, 855–861.

Li, J., and Tibshirani, R. (2013). Finding consistent patterns: a nonparametric approach for identifying differential expression in RNA-Seq data. Stat. Methods Med. Res. *22*, 519–536.

Liao, X.H., and Nguyen, H. (2014). Epidermal expression of Lgr6 is dependent on nerve endings and Schwann cells. Exp. Dermatol. *23*, 195–198.

Lien, W.H., Polak, L., Lin, M., Lay, K., Zheng, D., and Fuchs, E. (2014). In vivo transcriptional governance of hair follicle stem cells by canonical Wnt regulators. Nat. Cell Biol. *16*, 179–190.

Lim, X., Tan, S.H., Koh, W.L., Chau, R.M., Yan, K.S., Kuo, C.J., van Amerongen, R., Klein, A.M., and Nusse, R. (2013). Interfollicular epidermal stem cells self-renew via autocrine Wnt signaling. Science *342*, 1226–1230.

Lopez-Garcia, C., Klein, A.M., Simons, B.D., and Winton, D.J. (2010). Intestinal stem cell replacement follows a pattern of neutral drift. Science *330*, 822–825.

Mascré, G., Dekoninck, S., Drogat, B., Youssef, K.K., Broheé, S., Sotiropoulou, P.A., Simons, B.D., and Blanpain, C. (2012). Distinct contribution of stem and progenitor cells to epidermal maintenance. Nature *489*, 257–262.

Müller-Röver, S., Handjiski, B., van der Veen, C., Eichmüller, S., Foitzik, K., McKay, I.A., Stenn, K.S., and Paus, R. (2001). A comprehensive guide for the accurate classification of murine hair follicles in distinct hair cycle stages. J. Invest. Dermatol. *117*, 3–15.

Nakagawa, T., Nabeshima, Y., and Yoshida, S. (2007). Functional identification of the actual and potential stem cell compartments in mouse spermatogenesis. Dev. Cell *12*, 195–206.

Nowak, J.A., Polak, L., Pasolli, H.A., and Fuchs, E. (2008). Hair follicle stem cells are specified and function in early skin morphogenesis. Cell Stem Cell *3*, 33–43.

Page, M.E., Lombard, P., Ng, F., Göttgens, B., and Jensen, K.B. (2013). The epidermis comprises autonomous compartments maintained by distinct stem cell populations. Cell Stem Cell *13*, 471–482.

Petersson, M., Brylka, H., Kraus, A., John, S., Rappl, G., Schettina, P., and Niemann, C. (2011). TCF/Lef1 activity controls establishment of diverse stem and progenitor cell compartments in mouse epidermis. EMBO J. *30*, 3004–3018.

Rompolas, P., and Greco, V. (2014). Stem cell dynamics in the hair follicle niche. Semin. Cell Dev. Biol. *25-26*, 34–42.

Schepeler, T., Page, M.E., and Jensen, K.B. (2014). Heterogeneity and plasticity of epidermal stem cells. Development *141*, 2559–2567.

Silva-Vargas, V., Lo Celso, C., Giangreco, A., Ofstad, T., Prowse, D.M., Braun, K.M., and Watt, F.M. (2005). Beta-catenin and Hedgehog signal strength can specify number and location of hair follicles in adult epidermis without recruitment of bulge stem cells. Dev. Cell *9*, 121–131.

Simons, B.D., and Clevers, H. (2011). Strategies for homeostatic stem cell self-renewal in adult tissues. Cell *145*, 851–862.

Snippert, H.J., Haegebarth, A., Kasper, M., Jaks, V., van Es, J.H., Barker, N., van de Wetering, M., van den Born, M., Begthel, H., Vries, R.G., et al. (2010a). Lgr6 marks stem cells in the hair follicle that generate all cell lineages of the skin. Science *327*, 1385–1389.

Snippert, H.J., van der Flier, L.G., Sato, T., van Es, J.H., van den Born, M., Kroon-Veenboer, C., Barker, N., Klein, A.M., van Rheenen, J., Simons, B.D., and Clevers, H. (2010b). Intestinal crypt homeostasis results from neutral competition between symmetrically dividing Lgr5 stem cells. Cell *143*, 134–144.

Veniaminova, N.A., Vagnozzi, A.N., Kopinke, D., Do, T.T., Murtaugh, L.C., Maillard, I., Dlugosz, A.A., Reiter, J.F., and Wong, S.Y. (2013). Keratin 79 identifies a novel population of migratory epithelial cells that initiates hair canal morphogenesis and regeneration. Development *140*, 4870–4880.

Watt, F.M., and Hogan, B.L. (2000). Out of Eden: stem cells and their niches. Science *287*, 1427–1430.

Stem Cell Reports, Volume *5*

Supplemental Information

Dynamics of *Lgr6*$^+$ Progenitor Cells in the Hair Follicle, Sebaceous Gland, and Interfollicular Epidermis

Anja Füllgrabe, Simon Joost, Alexandra Are, Tina Jacob, Unnikrishnan Sivan, Andrea Haegebarth, Sten Linnarsson, Benjamin D. Simons, Hans Clevers, Rune Toftgård, and Maria Kasper

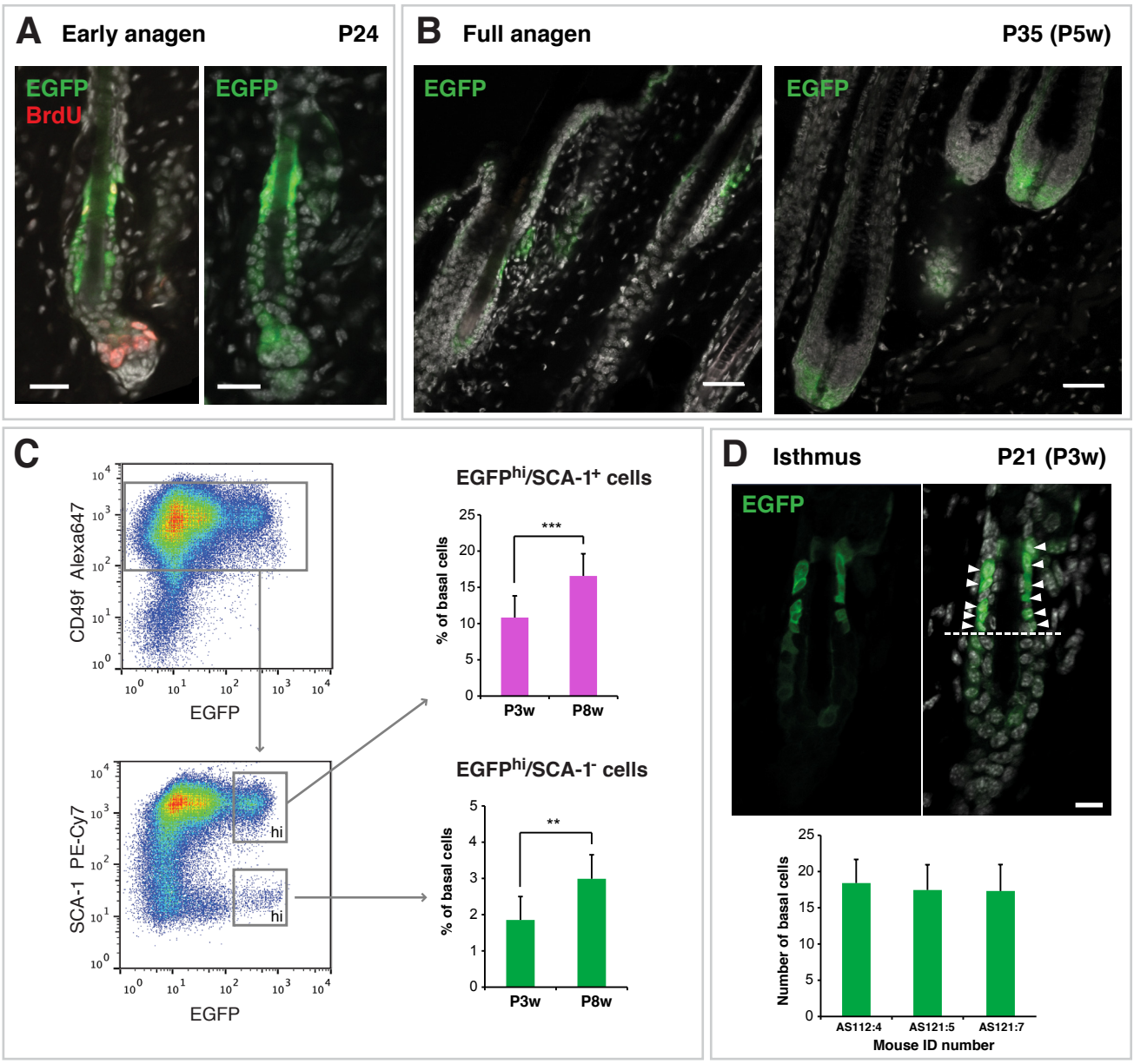
A
Early anagen
P24
EGFP
BrdU
EGFP
B
Full anagen
P35 (P5w)
EGFP
EGFP
C
CD49f Alexa647
EGFP
SCA-1 PE-Cy7
EGFP
hi
hi
EGFP^hi/SCA-1+ cells
% of basal cells
***
P3w
P8w
EGFP^hi/SCA-1- cells
% of basal cells
**
P3w
P8w
D
Isthmus
P21 (P3w)
EGFP
Number of basal cells
AS112:4
AS121:5
AS121:7
Mouse ID number

Figure S1

Figure S1. *Lgr6* expression during anagen and quantification of *Lgr6*$^{+}$ cells, related to Figure 1.

(A) Staining in skin of *Lgr6-EGFP-Ires-CreERT2* mice with anti-EGFP and anti-BrdU after a 2-hour BrdU pulse at the early anagen stage displays BrdU incorporation and EGFP expression in the expanding hair germ (n = 3 mice). Staining with anti-EGFP/anti-BrdU (left panel) and anti-EGFP only (right panel) are shown because BrdU-staining pretreatment lowers the anti-EGFP signal.
(B) EGFP antibody staining in skin of *Lgr6-EGFP-Ires-CreERT2* mice in anagen exhibits EGFP expression at the same sites as in telogen skin in the upper part of the PSU (left panel) and additional EGFP expression in the proximal anagen HF (right panel) (n = 3 mice).
(C) FACS quantification of EGFP expressing cells. Keratinocytes were isolated from skin of *Lgr6-EGFP-Ires-CreERT2* mice at P3w or P8w and stained with anti-CD49f and anti-SCA-1 antibodies to select for basal cells (CD49f^{+}) and discriminate IFE cells (SCA-1^{+}). The percentage of EGFP^{hi} cells was determined in the SCA-1^{+} and SCA-1^{-} basal fraction (P3w: n = 11 mice; P8w: n = 7 mice).
(D) Quantification of *Lgr6*^{IST} cells per PSU in P3w telogen skin. EGFP-antibody stained isthmus cells in skin of *Lgr6-EGFP-Ires-CreERT2* mice were counted in consecutive z-planes covering the entire isthmus in diameter (n = 3 mice; ≥ 7 entire HFs per mouse). Dashed line marks the bulge-isthmus border and arrowheads indicate the EGFP-expressing isthmus cells considered for *Lgr6*^{IST} quantification.
TO-PRO-3 nuclear stain (A, B and D). Scale bars, 25 μm (A), 50 μm (B), 10 μm (D).

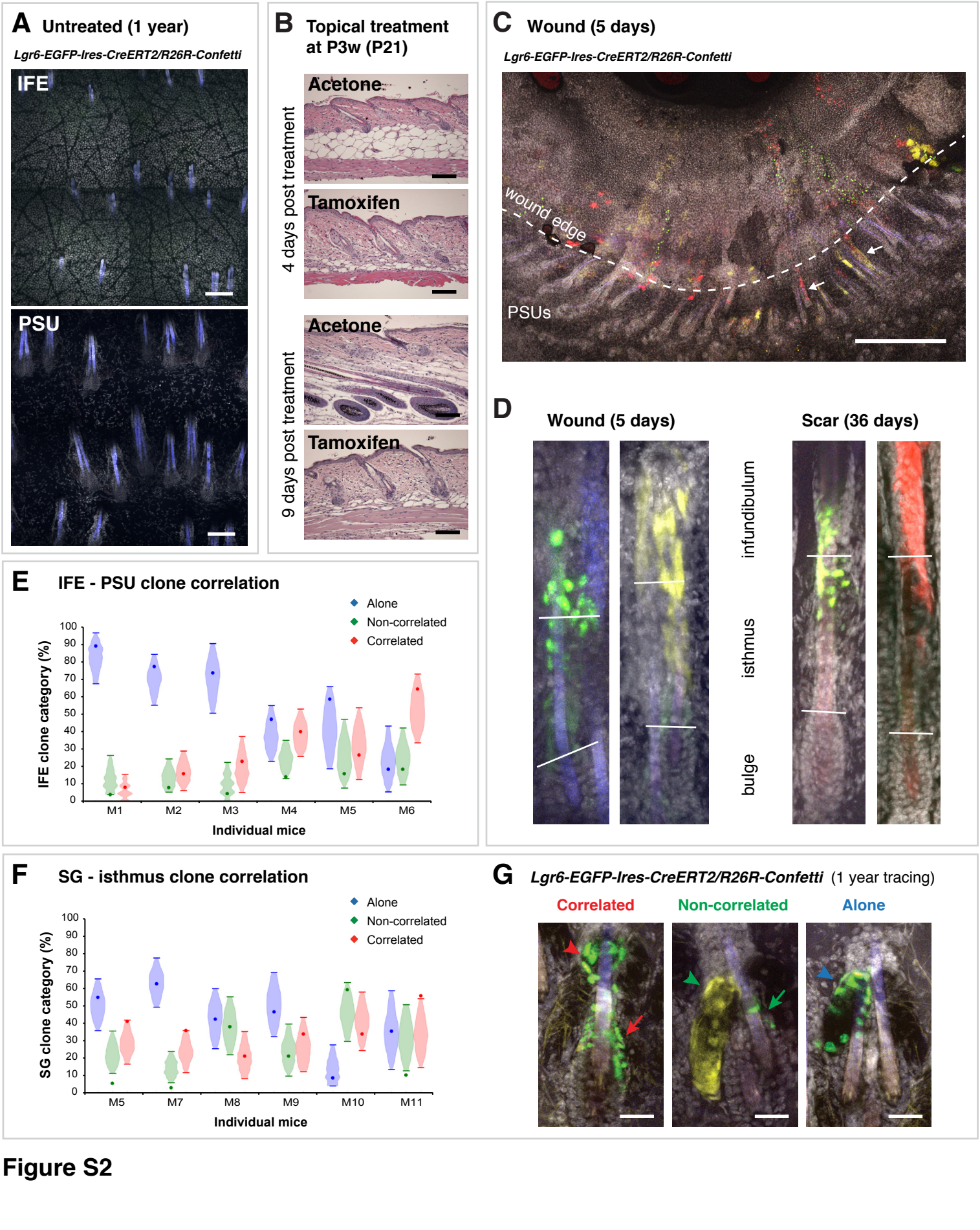
A Untreated (1 year)
Lgr6-EGFP-Ires-CreERT2/R26R-Confetti
IFE
PSU
B Topical treatment at P3w (P21)
4 days post treatment
Acetone
Tamoxifen
9 days post treatment
Acetone
Tamoxifen
C Wound (5 days)
Lgr6-EGFP-Ires-CreERT2/R26R-Confetti
wound edge
PSUs
D
Wound (5 days)
Scar (36 days)
infundibulum
isthmus
bulge
E IFE - PSU clone correlation
Alone
Non-correlated
Correlated
IFE clone category (%)
100
90
80
70
60
50
40
30
20
10
0
M1
M2
M3
M4
M5
M6
Individual mice
F SG - isthmus clone correlation
Alone
Non-correlated
Correlated
SG clone category (%)
100
90
80
70
60
50
40
30
20
10
0
M5
M7
M8
M9
M10
M11
Individual mice
G Lgr6-EGFP-Ires-CreERT2/R26R-Confetti (1 year tracing)
Correlated
Non-correlated
Alone

Figure S2

Figure S2. *Lgr6-EGFP-Ires-CreERT2/R26R-Confetti* lineage tracing during wound healing, and clone correlation between IFE-PSU and SG-IST, related to Figure 2.

(A) Representative z-stack projections of IFE and PSUs from a non-treated *Lgr6-EGFP-Ires-CreERT2/R26R-Confetti* mouse aged one year, demonstrating complete absence of labeling without tamoxifen (n = 3 mice). Hair shafts show autofluorescence in the blue channel.
(B) Hematoxylin/eosin stained sections from skin of *Lgr6-EGFP-Ires-CreERT2/R26R-Confetti* mice 4 and 9 days after topical treatment with tamoxifen or vehicle (acetone) at P3w. Tamoxifen-treated skin shows a delay in anagen induction compared to control skin (n = 3 mice).
(C) Representative whole mount image of a wound edge at day 5 after wounding in a *Lgr6-EGFP-Ires-CreERT2/R26R-Confetti* mouse treated with tamoxifen at P3w and wounded 4 days later (n = 3 mice). Arrows indicate the PSU clones contributing to IFE during wound closure.
(D) Representative confocal projections of $Lgr6^{PSU}$-traced clones in wound and scar environments in the dorsal skin demonstrate the survival of $Lgr6^{+}$ progeny in the infundibulum after wounding. Tamoxifen was given at P3w, wounds were made 4 days later, the wound tissue was analyzed 5 days after wounding (left panels, n = 3 mice), and the scar tissue was analyzed 36 days after wounding (right panels, n = 3 mice). Lines indicate the approximate borders between bulge, isthmus and infundibulum, and have a scale of 40 µm.
(E) Observed and expected percentages of "correlated", "non-correlated" and "alone" IFE clones compared to PSU clones. The observed percentages of each clone category are represented as dots. The expected percentages were estimated using a bootstrapping strategy assuming that IFE and PSU clones are not related (see Supplemental Experimental Procedures). The violin plots show the 95% confidence intervals of the expected percentages for each clone category and mouse. Note, in all mice and categories (18 out of 18), the observed values lay within the expected distribution, which implies that the IFE and the PSU clones are independent. The same mice and observed clone-categories as shown in Figure 2D and 2E were used. In total, 186 IFE clones and 875 PSUs were analyzed in 6 mice, which were traced for ≥40 days.
(F) Observed and expected percentages of "correlated", "non-correlated" and "alone" SG clones compared to isthmus clones. SG clones were assigned as shown in (G). The observed percentages of each clone category are represented as dots. The expected percentages were estimated using a bootstrapping strategy assuming that SG and isthmus clones are not related (see Supplemental Experimental Procedures). The violin plots show the 95% confidence intervals of the expected percentages for each clone category and mouse. Most of the observed values (14 out of 18) lay within the expected distribution, which is suggestive for independent compartment maintenance of isthmus and SG; however, a minor cellular exchange cannot be ruled out. In total, 165 SG clones were analyzed in 6 mice, which were traced for ≥40 days.
(G) Illustrative pictures of *Lgr6-EGFP-Ires-CreERT2/R26R-Confetti* mouse skin that was traced for 1 year showing SG clones that are isthmus-correlated (red arrowhead), non-correlated (green arrowhead) or alone (blue arrowhead).
Confetti clone colors in nuclear green, yellow, red and membranous blue (A, C, D and G), TO-PRO-3 nuclear stain in gray (A and C, D and G). Scale bars, 100 µm (A and B), 500 µm (C), 40 µm (D), 25 µm (G).

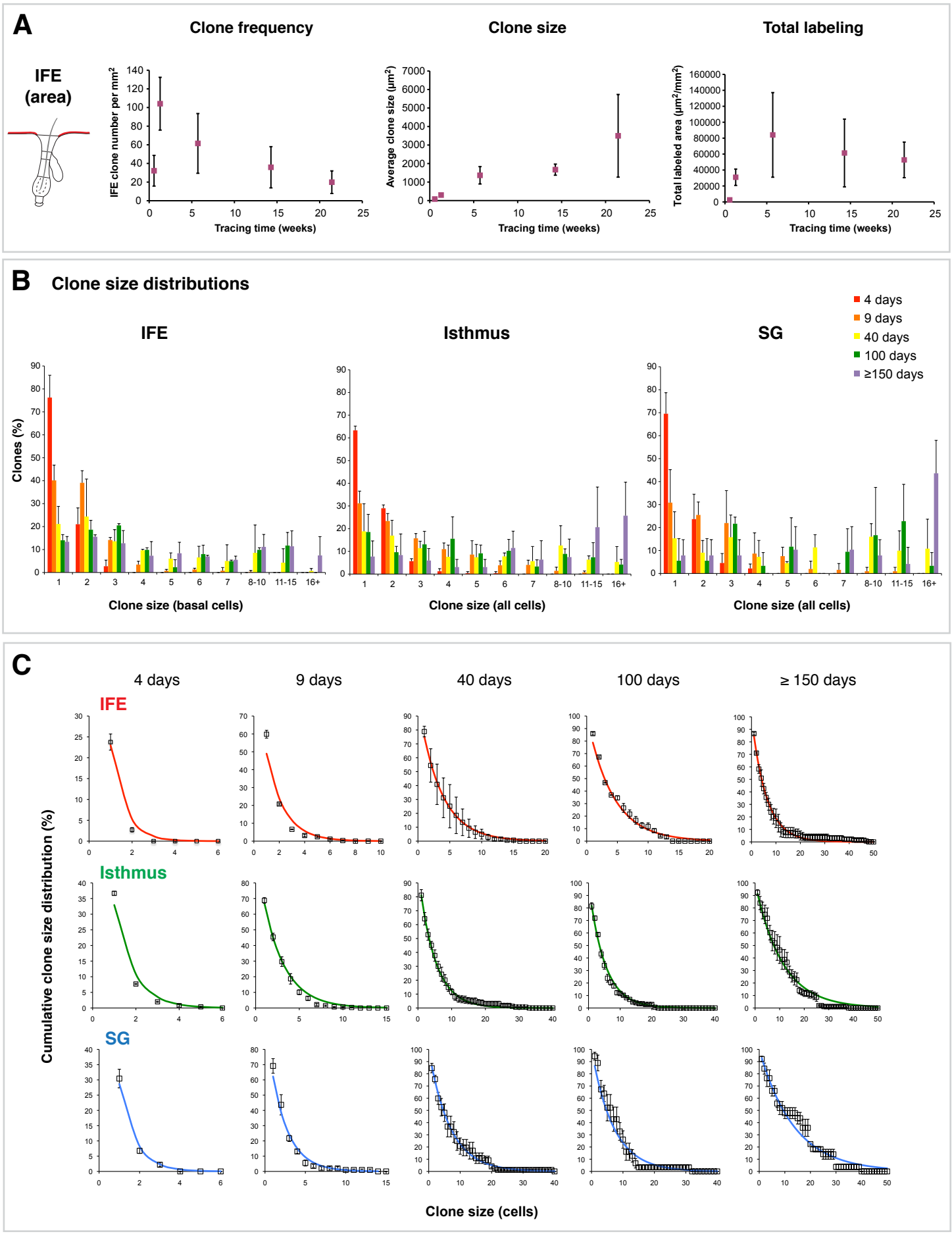
A
Clone frequency
Clone size
Total labeling
IFE (area)
IFE clone number per mm²
Average clone size (µm²)
Total labeled area (µm²/mm²)
Tracing time (weeks)
B
Clone size distributions
IFE
Isthmus
SG
4 days
9 days
40 days
100 days
≥150 days
Clones (%)
Clone size (basal cells)
Clone size (all cells)
C
4 days
9 days
40 days
100 days
≥ 150 days
IFE
Isthmus
SG
Cumulative clone size distribution (%)
Clone size (cells)

Figure S3

Figure S3. *Lgr6*$^+$ clone dynamics and clone size distributions, related to Figure 3.

(A) *Lgr6-EGFP-Ires-CreERT2/R26R-Confetti* clone dynamics in the IFE was additionally measured by determining the total area of the clones in z-stack projections of flat-mount images. The average IFE clone number is higher than in the basal-cell clone analysis due to inclusion of clones without basal cells. Similar dynamics of decreasing clone frequency and increasing clone size were confirmed. The total labeled area reached the highest level only after 5.5 weeks tracing as the clones of earlier time points consisted mostly of basal cells.
(B) Histograms displaying the percentage of clones of different sizes (numbers of cells) in IFE, isthmus and SG. The clone size distributions become broader with time.
(C) Cumulative clone size distributions in IFE, isthmus and SG show an exponential shape matching the predictions of the committed progenitor model. At clone size n, the chance of finding a surviving *Lgr6*$^+$-derived clone with more than n cells is shown.
Data are shown as mean of 3 mice ± SD (A and B) or ± SEM (C).

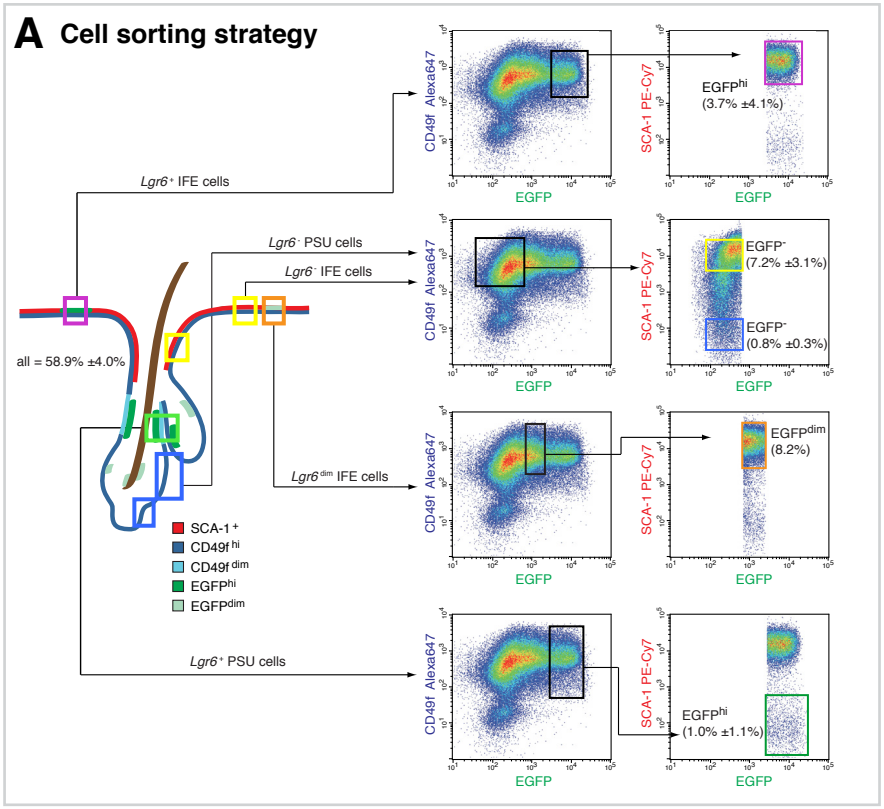
A Cell sorting strategy
Lgr6+ IFE cells
Lgr6- PSU cells
Lgr6- IFE cells
Lgr6dim IFE cells
Lgr6+ PSU cells
all = 58.9% ±4.0%
SCA-1+
CD49fhi
CD49fdim
EGFPhi
EGFPdim
CD49f Alexa647
SCA-1 PE-Cy7
EGFP
EGFPhi (3.7% ±4.1%)
EGFP- (7.2% ±3.1%)
EGFP- (0.8% ±0.3%)
EGFPdim (8.2%)
EGFPhi (1.0% ±1.1%)

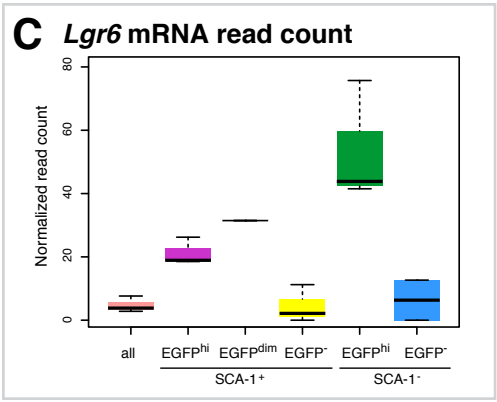
C Lgr6 mRNA read count
Normalized read count
all
EGFPhi
EGFPdim
EGFP-
EGFPhi
EGFP-
SCA-1+
SCA-1-

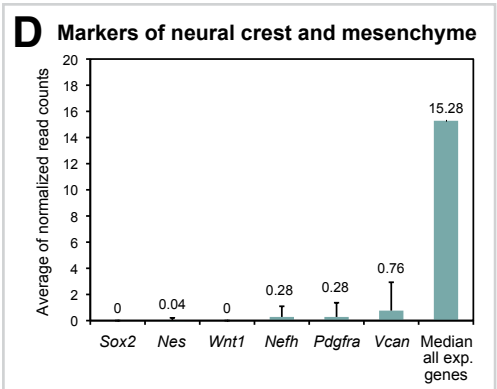
D Markers of neural crest and mesenchyme
Average of normalized read counts
0
0.04
0
0.28
0.28
0.76
15.28
Sox2
Nes
Wnt1
Nefh
Pdgfra
Vcan
Median all exp. genes

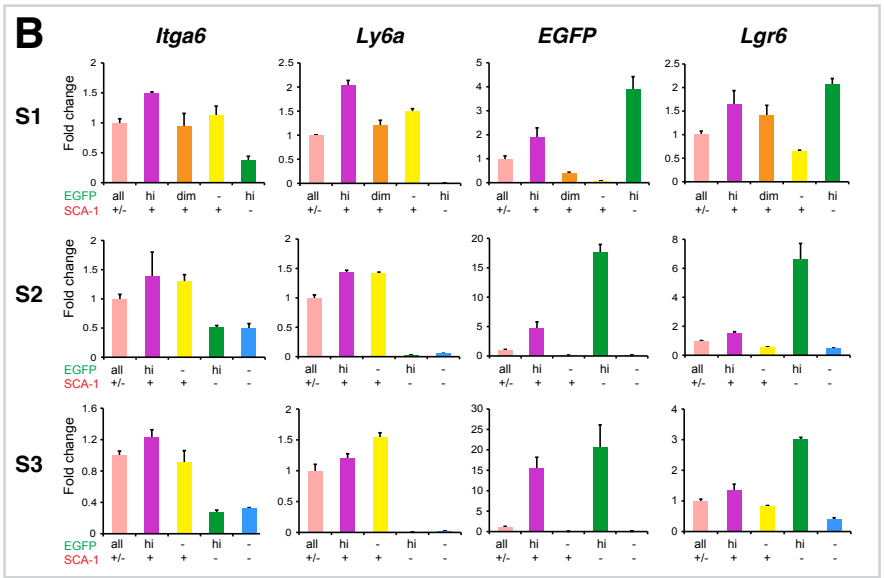
B
Itga6
Ly6a
EGFP
Lgr6
S1
S2
S3
Fold change
EGFP
SCA-1
all
hi
dim
-

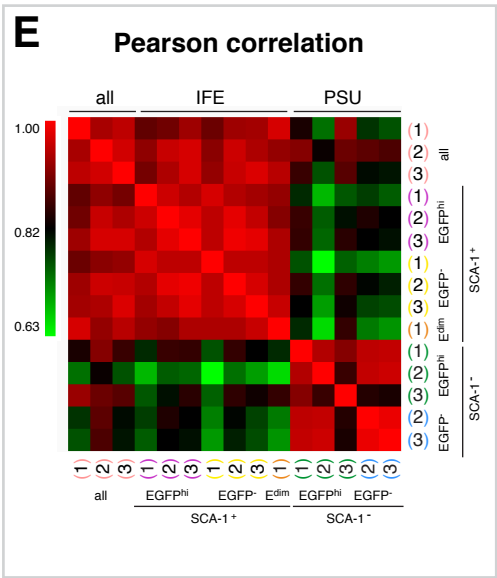
E Pearson correlation
all
IFE
PSU
1.00
0.82
0.63
EGFPhi
EGFP-
Edim
SCA-1+
SCA-1-

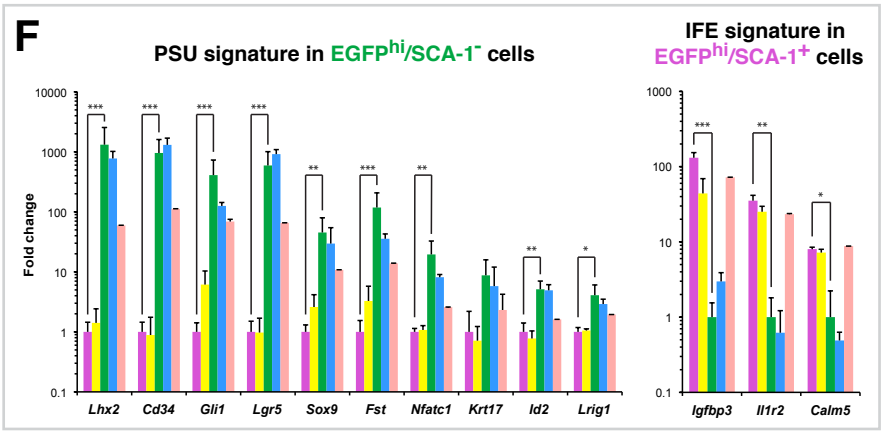
F
PSU signature in EGFPhi/SCA-1- cells
IFE signature in EGFPhi/SCA-1+ cells
Fold change
Lhx2
Cd34
Gli1
Lgr5
Sox9
Fst
Nfatc1
Krt17
Id2
Lrig1
Igfbp3
Il1r2
Calm5

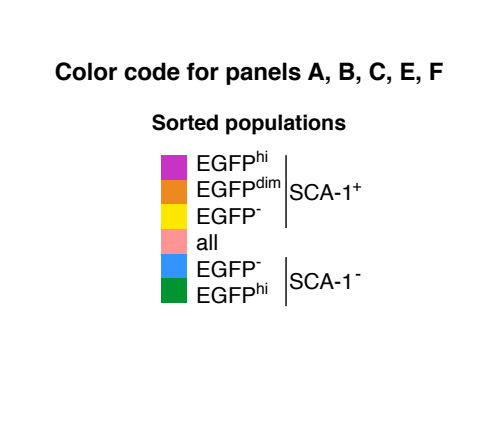
Color code for panels A, B, C, E, F
Sorted populations
EGFPhi
EGFPdim
EGFP-
all
EGFP-
EGFPhi
SCA-1+
SCA-1-

Figure S4

Figure S4. RNA-seq analysis of FACS-sorted *Lgr6*$^{+}$ and *Lgr6*$^{-}$ keratinocyte populations, related to Figure 4.

(A) Scheme illustrating the sorting strategy for the different keratinocyte populations used for RNA-seq analysis, including illustrative FACS plots of all sorted keratinocyte populations. The size of the populations is represented as a percentage of all measured (ungated) cells ± SD.
(B) Real-time PCR analysis of the sorting markers CD49f (*Itga6*), SCA-1 (*Ly6a*) and EGFP was used to validate the purity of the populations in each sorting (S1–S3), and *Lgr6* expression was measured to display the relative levels of *Lgr6* and *EGFP* mRNA expression in the respective sorted samples. Data are shown as mean of three technical replicates (± SD) assayed in each of the three independent sortings.
(C) Boxplots showing normalized *Lgr6* mRNA reads in the different populations, measured by RNA-seq and normalized using DESeq, which confirms that the *Lgr6* mRNA levels were in agreement with EGFP protein levels.
(D) Mean normalized RNA-seq read counts (of all sorted samples) of genes associated with mesenchymal or neural origin. For comparison, the median read count of all expressed genes (read count >0) is presented. The absence or very low read counts for these marker genes ruled out contamination of the sorted populations by non-epithelial cells.
(E) Heatmap showing Pearson correlations across all genes, pairwise for all samples from the three independent cell sortings.
(F) Real-time PCR analysis of selected genes that represent the transcriptional PSU- or IFE-phenotype of EGFP^{hi}/SCA-1^{-} and EGFP^{hi}/SCA-1^{+} cells, respectively. Data are shown as mean of ≥ 2 biological replicates ± SD. Significance tests were performed between EGFP^{hi}/SCA-1^{-} and EGFP^{hi}/SCA-1^{+} populations (n = 3 biological replicates). Asterisks indicate T-test significance level at $p<0.05$ (*), $p<0.01$ (**) and $p<0.001$ (***).

SUPPLEMENTAL TABLES

Table S1. Comparison of the observed with the expected frequencies of Confetti-clone colors in IFE and PSU, related to Figure 2.

Mouse ID	AS30:5 (M4)	AS30:7 (M3)	AS42:3 (M6)	AS55:2 (M5)	AS51:4 (M2)	AS55:3 (M1)
Correlated $_{observed}$	0.395	0.227	0.636	0.263	0.158	0.080
μ (Correlated $_{simulated}$)	0.333	0.197	0.552	0.373	0.180	0.065
2σ (Correlated $_{simulated}$)	0.169	0.143	0.178	0.174	0.137	0.088
Non correlated $_{observed}$	0.140	0.0455	0.182	0.158	0.079	0.040
μ (Non correlated $_{simulated}$)	0.220	0.157	0.243	0.231	0.146	0.061
2σ (Non correlated $_{simulated}$)	0.149	0.131	0.154	0.151	0.127	0.086
No label $_{observed}$	0.465	0.727	0.182	0.579	0.763	0.880
μ (No label $_{simulated}$)	0.447	0.646	0.204	0.397	0.674	0.874
2σ (No label $_{simulated}$)	0.179	0.172	0.145	0.176	0.168	0.119

Table S2. *Lgr6-EGFP-Ires-CreERT2/R26R-Confetti* mice and clones evaluated for each time point, related to Figure 3.

	4 days					9 days				40 days			100 days			≥ 150 days			
Mouse ID (AS no.)	42:1	42:6	45:2	48:2	48:3	42:6	45:2	48:2	157:1	51:1	90:7	152:7	42:2	51:2	122:3	42:1	51:4	90:4	122:6
Days traced	4	4	4	4	4	9	9	9	9	40	41	39	99	103	101	143	194	160	149
HFs counted	NA	NA	73	110	92	NA	76	70	57	98	85	101	94	73	52	100	179	65	NA
Total HF clones	NA	NA	81	121	114	NA	140	136	87	109	76	153	76	21	71	56	14	53	NA
Total labeled HF cells	NA	NA	109	179	164	NA	399	367	213	742	258	723	498	114	308	394	173	441	NA
Isthmus clones	NA	NA	43	88	74	NA	95	89	56	54	38	97	54	15	45	38	5	30	NA
Total labeled isthmus cells	NA	NA	62	134	108	NA	308	259	133	431	154	453	320	72	227	260	75	319	NA
SG clones	NA	NA	25	27	35	NA	25	34	21	27	21	20	10	5	12	8	5	9	NA
Total labeled SG cells	NA	NA	32	39	51	NA	47	91	59	192	58	188	86	33	46	93	77	101	NA
IFE clones	32	27	62	17	68	110	144	141	NA	90	290	91	80	23	82	72	66	75	32
IFE basal clones	32	27	62	17	66	84	104	118	NA	64	NA	70	65	20	NA	60	NA	68	32
Total labeled IFE cells	36	31	81	24	88	173	205	212	NA	158	NA	375	291	101	NA	296	NA	610	572
HF clone color distribution																			
Blue (%)	NA	NA	1.2	0.0	3.5	NA	6.4	11.8	37.9	0.0	21.1	11.8	0.0	0.0	15.5	0.0	0.0	11.3	NA
Green (%)	NA	NA	6.2	1.7	6.1	NA	9.3	20.6	29.9	15.6	0.0	32.0	2.6	0.0	28.2	0.0	7.1	3.8	NA
Yellow (%)	NA	NA	42.0	48.3	45.6	NA	40.7	33.1	28.7	35.9	40.8	29.4	46.8	52.4	29.6	53.6	50.0	34.0	NA
Red (%)	NA	NA	50.6	50.0	44.7	NA	45.7	33.8	3.4	48.4	38.2	28.1	50.6	47.6	26.8	46.4	42.9	50.9	NA

Table S3. Primers for cDNA amplification, related to Figures 4 and S4.

The primers were optimized for the following conditions: 5 min at 94 °C initial denaturation, 10 cycles of [1 min at 94 °C denaturation, 1 min at 60 °C annealing, and 2 min at 72 °C extension].

Gene	Forward primer sequence 5'-3'	Reverse primer sequence 5'-3'
Alcam	TTGTGGGAATTGTCGTTGGTCT	CAATCCACGTTCATGCTTCAAT
Calm5	AATGAAGCAGTTGGGCAAGAAC	CAAAAACTGCTCATAGTTCACCTTCC
Cd34	CCACTTCAGAGATGACCTGGAA	GGCTAGAAGCAGGGAGCAGA
Cd44	GAACAGGACAGGACCACTTTCA	CCTGGTAAGGAGCCATCAACAT
Cst6	TAGAAAGCACAGAGTGCCGAAA	AGGAGAAAGCAGTGCAAGAAGC
Defb6	CCTGCTCTTTGCCTTTATCCTG	GATTTTAGGATGGCCACAATGGC
EGFP	ATGGCCGACAAGCAGAAGAA	GTCCATGCCGAGAGTGATCC
Fst	GGAAAACCTACCGCAACGAAT	TTCAGAAGAGGAGGGCTCTGG
Fzd1	CTCGCCAGCCACTGACTTTT	GCAGAAAAGGGCAAGTGAGAAA
Gli1	GCCGCCTGGAGAACCTTAG	GGTAGTGACGATGCCCCATT
Hprt1	GGGGGCTATAAGTTCTTTGC	TCCAACACTTCGAGAGGTCC
Id2	GACCCGATGAGTCTGCTCTAC	TTCGACATAAGCTCAGAAGGGAAT
Igfbp3	TCAAAGCACAGACACCCAGAAC	CACGGAGCATCTACTGGCTCT
Il1r2	ATACCAGCATCATTGGGGTCA	TCCAGGAGAACGTGGAAGAGA
Itga6	TCAGGAGTAGCTTGGTGGATCA	CGAGGTTATCCATGTGTTTCTCA
Krt14	CACCATGCAGAACCTGGAGAT	TGGATGACTGAGAGCCAGAGG
Krt17	GCAGAACCAGGAGTACAAGATCC	GCTGTAGCAGGAGGGTGATG
Lgr5	CCGAGCCTTACAGAGCCTGA	AGGTGCTCACAGGGCTTGAA
Lgr6	TCAGGGAACCACCTCTCACAC	TGGAAGGCATAGTCAGGGATG
Lhx2	GTCTATTGCCGCTTGCACTTC	GTCTTTTGGCTGCTGGGGTAG
Lrig1	GGTCCCTCTATCCAAGCAACC	TCCCAGTGATCTGCCCTTTC
Ly6a	CTCAGGGACTGGAGTGTTACC	GCAGAGGTCTTCCTGGCAAC
Nfatc1	AGCCCCGTCCAAGTCAGTTT	GCAGGAGAGGAAAGGTCGTG
Nrp1	CAACTGGTCTGGATGGTGGTT	TAAGCACATTGCCTGGCTTC
Pthlh	GGTTTGAGAGAGGCGCAGTT	TCTGATTTCGGCTGTGTGGA
Rplp0	CCTGAAGTGCTCGACATCACA	CCTCCGACTCTTCCTTTGCT
Sostdc1	TCCTCCTGCCATTCATCTCTC	CATAGCCTCCTCCGATCCAGT
Sox4	TGCCTCATGGTCAAGAAAGGA	GCTACTCCCAGCACATCTCCA
Sox9	AGGTGCTGAAGGGCTACGACT	CCGGGGCTGGTACTTGTAATC
Tcf7l2	AACCCTCAAGGATGCTCGTTC	TCCTCCTGTCGTGATTGGGTA
Tnfrsf19	CAATGTATGGGCCTGTTCACCT	CGGGATTGAGGGAATTGGTATC
Wnt6	CTCCAGGACCAACTGGCTCTC	AGAGCTTTGCCGTCGTTGGTG

Table S4. Primers for qPCR, related to Figures 4 and S4.

The primers were optimized for the following conditions: 3 min at 95 °C initial denaturation, 42 cycles of [15 s at 95 °C denaturation, 15 s at 65 °C annealing, and 30 s at 72 °C extension].

Gene	Forward primer sequence 5'-3'	Reverse primer sequence 5'-3'
Alcam	CCTCGTTGCTGGTGTCGTCTACTGG	CAGGCTATCCAATCCGCTCCTCTCT
Calm5	GCAGGCTATGTTCAGTGTCCTTGACC	TTCACCTTCCCATCTTGGTCTGCAC
Cd34	GATGACATCACCCACCGAGCCATA	CCTCAGCCTCCTCCTTTTCACACAG
Cd44	GGAGAGCCGGAAGAAGACGAAAACC	AGCAGGGGTCACTGGGAAGAGAGTC
Cst6	ACATGGACCTCACCACCTGCCCTCT	GCTGAGTAGTGTTCTTCCAGGGGACTTCA
Defb6	ATCTCTGCACCTCACCAGGCATCAG	GCTGTCTCCACTTGCAGCCTTTTCC
EGFP	GATCCGCCACAACATCGAGGACG	GGCGGTCACGAACTCCAGCAG
Fst	GCACTCCTCAAGGCCAGATGCAAAG	CACAAGTGGAGCTGCCTGGACAAAA
Fzd1	CCCTTTCCCAACAAACAGCACAGGT	AGATCGGTCCACACGCACATACACA
Gli1	CCCATAGGGTCTCGGGGTCTCAAAC	GGAGGACCTGCGGCTGACTGTGTAA
Hprt1	CAACGGGGGACATAAAAGTTATTGGTGG	TGCAACCTTAACCATTTTGGGGCTGT
Id2	GGACTCGCATCCCACTATCGTCAGC	GGGAATTCAGATGCCTGCAAGGACAG
Igfbp3	AGGCGTCCACATCCCAAACTGTGAC	TCGTCTTTCCCCTTGGTGTCGTAGC
Il1r2	TGACCGAGGGGCTACACCACCAGTA	CTCCGTGGATTCGAGGCAACACATT
Itga6	CTGTTCTTGCCGGGATTCTGATGCT	GCATGGTATCGGGGAATGCTGTCAT
Krt14	TGCTGGATGTGAAGACAAGGCTGGA	GGAAGATGAAAGGTGGGCGTCCTCT
Krt17	AAGACAAGGCTGGAGCAGGAGATCG	GCTGAGTCCTTAACGGGTGGTCTGG
Lgr5	CCAATGGAATAAAGACGACGGCAACA	GGGCCTTCAGGTCTTCCTCAAAGTCA
Lgr6	CTGGACCCCCTGACGGCTTACCT	GATCCCACGGAGCTGGTTGCTCT
Lhx2	CCTACTACAACGGCGTGGGCACTGT	GTCACGATCCAGGTGTTCAGCATCG
Lrig1	GCAGATGGGAACGGAGATTCCTCTTG	TGCTGGGCTTCAGTAGATATGGCGTC
Ly6a	TGCCCCTACCCTGATGGAGTCTGTG	GGAGGGCAGATGGGTAAGCAAAGATTG
Nfatc1	ATGTCTGCAACGGGAAACGGAAGAG	AGGCATGGTGAGCTGTTGGCTGTAG
Nrp1	GGAAACCTTGGTGGAATTGCTGTGG	TCTTGTCACCTTCCCCTTCTCCTTCA
Pthlh	TGGTTCAGCAGTGGAGTGTCCTGGT	GATGGACTTGCCCTTGTCATGCAGT
Rplp0	TGCACTCTCGCTTTCTGGAGGGTGT	AATGCAGATGGATCAGCCAGGAAGG
Sostdc1	CCAGCAGCAACAGCACCCTGAATC	TGCACTGGCCGTCCGAAATGTAT
Sox4	CCATCTCCTACCCACCCCCTCTTTG	TTCTCCATGCCAATGCTCCCCTAAG
Sox9	CAGACCAGTACCCGCATCTGCACAA	AAGGGTCTCTTCTCGCTCTCGTTCAGC
Tcf7l2	TCACGCCTCTCATCACGTACAGCAA	CCTAGCGGATGGGGGATTTGTCCTA
Tnfrst19	GATTCCGTCCTTGTGCTGTGAAGAGG	GGAACGGGAAACAGACCCGAAGAAG
Wnt6	AGGCTGCGGAGACGATGTGGACTT	GCAGAGCGCAGGAACCCGAAAG

SUPPLEMENTAL EXPERIMENTAL PROCEDURES

Microscopy and image analysis

Imaging was performed using an LSM710-NLO confocal microscope (Zeiss) or a Nikon A1R confocal microscope. Confetti-color detection was carried out on the Zeiss microscope using 405-nm, 488-nm, 514-nm and 561-nm lasers for CFP, GFP, YFP and RFP/TO-PRO-3, respectively, and images were acquired with a 20x water-dipping objective at 1024x1024 resolution. Combinations of z-stack and tiling images were recorded using narrow filtering on spectral detectors to avoid bleed-through. Z-stack images of RNA *in situ* stainings were recorded with a z-distance of 0.65 µm using a 60x objective. Image analysis was performed using NIS-Elements software (Nikon), Zen 2009 software (Zeiss), or ImageJ, and images were occasionally optimized for brightness, contrast, and color balance.

Horizontal whole mount (HWM) IF staining

Samples of dorsal skin were fixed in 4% PFA for 20 min and mounted in OCT embedding medium (Histolab). Subsequently, 150-µm sections were cut with a cryostat, blocked with PB buffer (0.1% fish skin gelatin, 0.5% Triton X-100 and 0.5% skimmed milk powder in PBS) and stained as described previously (Driskell et al., 2009). The nuclear stain, TO-PRO-3 (Invitrogen, 1:1000), was applied at the same time as secondary antibodies (Alexa Fluor Dyes 488, 546, 647 or 680; Invitrogen, 1:500).

RNA *in situ* hybridization (ISH) on paraffin sections

ISH was performed on PFA-fixed and paraffin-embedded skin sections using the RNAscope Fluorescent Multiplex Kit (Advanced Cell Diagnostics, Inc.) according to the manufacturer's instructions. Critically, skin tissue sections were heat-pretreated for 15 min and underwent protease digestion for 30 min. The following RNAscope probes were used: *Lgr6* (ACD404961), *Defb6* (ACD430141) and *Krt5* (ACD415041). The housekeeping gene *Polr2a* served as a positive control whereas a probe targeting the bacterial mRNA *dapB* was used as a negative control on consecutive skin sections.

Real-time PCR

Real-time PCR was performed on the same RNA samples used for sequencing after pre-amplification of the cDNA with gene-specific, nested primers. Per sample, 2 ng RNA were reverse-transcribed using Superscript III First-Strand Synthesis Kit (Invitrogen) and gene-specific reverse primers for the outer nested PCR product. Then, gene-specific forward primers were added, and the cDNA was amplified for 10 cycles, generating the outer nested PCR products. The resulting amplified cDNA was analyzed with real-time PCR using a second pair gene-specific primers located within the sequence of the nested PCR fragment. The assays were run using Power SYBR Green PCR Master Mix on a 7900HT Fast Real-Time PCR system (both Applied Biosystems). All primers were designed to span exon boundaries using the Primer 3 online tool. Complete lists of primer sequences and PCR conditions are available in Tables S3 and S4.

Confetti clone definition and categorization

First, cohesively connected cells in the same color were defined as one clone. To place the cells within the distinct compartments of the PSU, we used anatomical features such as the SG-opening (demarcating the upper and lower border of the junctional zone), or the inner bulge cells to identify the lower border of the isthmus.

Figure 2. For the IFE – PSU correlation analysis, an IFE clone of a given color (e.g. red) was picked, and compared with every PSU surrounding the IFE clone in a radius of 150–200 µm. If there was at least one red clone in one of the surrounding PSUs, the IFE clone was categorized 'correlated'. If there was no red clone in these PSUs, but at least one clone in another color, the IFE clone was categorized 'non-correlated', and if none of the surrounding PSUs were labeled, the IFE clone was categorized 'alone'.
For the SG – isthmus correlation analysis, a SG clone of a given color (e.g. red) was picked, and compared with the lower isthmus of the same PSU. If there was at least one red clone in the lower isthmus (green area in Figure 2B), the SG clone was categorized as 'correlated'. If there was no red clone in the lower isthmus, but at least one clone in another color, the SG clone was categorized 'non-correlated', and if there was no clone in the lower isthmus, the SG clone was categorized 'alone'.
Figure 3. Isthmus clones were defined as having at least one cell in the lower isthmus (see Figure 2B, green area) and all cohesively connected cells of the same Confetti color were counted for quantification of the clone size. SG clones were defined as having at least one cell in the SG (see Figure 2B, blue area) and at the same time no connected cell of the same color in the lower isthmus area. All cohesively connected cells of the same Confetti color were used for SG clone size quantification.

Simulation strategy for IFE – PSU color correlation
The simulation analysis was performed using Python, and the scripts are available upon request. In order to simulate the expected IFE – PSU color correlation as a function of labeling efficiency (Figure 2E), under the assumption that IFE and PSU are independent compartments, we devised the following simulation model:

For each labeling efficiency ***L*** (from 0.05–1 in incremental steps of 0.05), we simulated 100.000 experiments. In each experiment, we assigned each of ***n_clones_IFE*** IFE clones with a color ***c_IFE***. We then chose a number of ***n_PSU*** surrounding PSUs for each IFE clone and subsequently determined the number of PSU clones ***n_clones_PSU*** in dependency of ***L*** for each PSU and the corresponding color ***c_PSU*** for each PSU clone. Next, we marked each IFE clone as 'correlated', 'non-correlated' or 'alone' depending on whether the surrounding PSUs carry a correlated clone, only uncorrelated clones or no clones at all. For each experiment, we return the fraction of IFE clones which were marked as 'correlated', 'non-correlated' or 'alone' and for each labeling efficiency, we return the mean and standard deviations of those values derived from 100.000 experiments.

The number ***n_clones_IFE*** of IFE clones simulated per experiment is based on the average number of IFE clones counted in each empirical experiment.

The number ***n_PSU*** of surrounding PSUs per IFE clone is randomly chosen from a Poisson distribution with a λ that reflects the average number of PSUs per IFE clone as observed over all empirical experiments. While the empirical distribution of HFs per IFE clone is slightly underdispersed compared to a Poisson distribution (data not shown), we regard it as a robust approximation.

The colors ***c_IFE*** and ***c_PSU*** for each IFE and PSU clone are randomly chosen based on the empirically determined color probabilities for IFE and PSU clones averaged over all empirical experiments.

We assumed that the number ***n_clones_PSU*** of clones per PSU – the most critical parameter in the simulation – could be derived from a discrete probability distribution in dependency of ***L***, which we define as average number of clones per PSU ***μ(n_clones_PSU)***. The empirical values for ***n_clones_PSU*** point to a distribution that is overdispersed compared to an ideal Poisson distribution (not shown). Such a distribution can be modeled as Gamma mixture of Poisson distributions. Hence

$n\_clones\_PSU \sim Poisson(\lambda) \qquad \lambda \sim Gamma(k, \theta)$

with

$\mu(n\_clones\_PSU) = L = k\,\theta \qquad \sigma(n\_clones\_PSU) = k\,\theta\,(1+\theta)$

We noted that in the empirical data, the variance ***σ(n_clones_PSU)*** scales linearly with the mean ***μ(n_clones_PSU***) = *L* and can thus be expressed as

$\sigma(n\_clones\_PSU) = r\,\mu(n\_clones\_PSU) = r\,L$

where ***r*** is an empirically determined dispersion factor. While a Gamma-Poisson mixture with $k = L / (r - 1)$ and $\theta = r - 1$ would perfectly model mean and variance of our empirical data, we noted that a Gamma-Poisson mixture with k = L / r and $\theta = r$ – while overstating the variance – provides an overall better fit to the empirically determined distribution of clones per PSU in dependency of *L*. We reason that the empirical distribution is truncated due to the limited space for clones in the isthmus and SG regions of the PSU and thus exhibits a lower variance compared to an ideal Gamma-Poisson distribution. We thus chose

$n_{IST} \sim Poisson(\lambda) \qquad \lambda \sim Gamma(L / r\,,\, r)$

as our final model.

Resampling strategy for IFE – PSU and SG – IST color correlation

As an alternative approach, we used bootstrapping methodology to infer the expected numbers of 'correlated', 'non-correlated' and 'alone' clones if **(a) IFE – PSU** and **(b) SG – IST** were independent compartments. In contrast to the simulation approach specified above, this resampling approach has the advantage that it does not rely on assumptions about the underlying distributions for each parameter but instead only uses the empirical data. The bootstrapping analysis was performed using Python, and the scripts are available upon request.

For each mouse analyzed in **(a) Figure S2E** and **(b) Figure S2F**, we extracted and employed following empirical data:

- **(a)** ***clones_per_IFE*** or **(b)** ***clones_per_SG*** (the number of IFE clones in all analyzed fields-of-view for **(a)** or the number of SG clones in all analyzed PSUs for **(b)**).

- **(a)** ***c_IFE*** or **(b)** ***c_SG*** (the number of B, G, Y, R clones among all IFE clones for **(a)** or the number of B (blue), G (green), Y (yellow), R (red) clones among all SG clones for **(b)**).

- **(a)** ***clones_PSU*** or **(b)** ***clones_IST*** (the number of all PSU clones over all analyzed fields-of-view for **(a)** or the number of IST clones in all analyzed PSUs for **(b)**).

- **(a)** ***c_PSU*** or **(b)** ***c_IST*** (the number of B, G, Y, R clones among all PSU clones for **(a)** or the number of B, G, Y, R clones among all IST clones for **(b)**).

- **(a)** ***n_replicates_IFE*** or **(b)** ***n_replicates_SG*** (number of times an IFE clone was detected and compared to the surrounding PSUs in the empirical data for **(a)** or the number of times an SG clone was detected and correlated to the adjacent isthmus in the empirical data for **(b)**; corresponds to the number of replicates in each mouse).

We then randomly sampled with replacement from the specified empirical data using the following approach:

1. Sample once from ***clones_per_IFE*** or ***clones_per_SG*** to get an IFE clone number ***n_IFE*** for **(a)** or an SG clone number ***n_SG*** for **(b)**.

2. Sample ***n_IFE***-times from ***c_IFE*** or ***n_SG***-times from ***c_SG*** to assign a color to each IFE clone for **(a)** or each SG clone for **(b)**.

3. Sample once from ***clones_per_PSU*** or ***clones_per_IST*** to get a PSU clone number ***n_PSU*** for **(a)** or an IST clone number ***n_IST*** for **(b)**.

4. Sample ***n_PSU***-times from ***c_PSU*** or ***n_IST***-times from ***c_IST*** to assign a color to each PSU clone for **(a)** or each IST clone for **(b)**.

5. Compare each randomly colored IFE clone to each of the respective PSU clones for **(a)** or each randomly colored SG clone to each clone in the respective IST **(b)**. Count a **correlation** event if at least one PSU clone **(a)** / IST clone **(b)** has the same color as the IFE clone **(a)** / SG clone **(b)**. Count a **non-correlation** event if no PSU clone **(a)** / IST clone **(b)** has the same color as the IFE clone **(a)** / SG clone **(b)**. Count an **alone** event if the number of PSU **(a)** / IST **(b)** clones is equal to 0.

6. Repeat steps 1 – 5 ***n_replicates_IFE***-times for **(a)** or ***n_replicates_SG***-times for **(b)** that equals the number of replicates of the empirical data analysis for each mouse. Return the relative values for **correlation**, **non-correlation** and **alone** events.

7. Repeat steps 1 – 6 **1000**-times to yield a distribution of relative values of **correlation**, **non-correlation** and **alone** events which reflects the expected null distribution if there is no exchange between compartments.

SUPPLEMENTAL REFERENCE

Driskell, R.R., Giangreco, A., Jensen, K.B., Mulder, K.W., and Watt, F.M. (2009). Sox2-positive dermal papilla cells specify hair follicle type in mammalian epidermis. Development *136*, 2815-2823.